

# The Formation of Disk Galaxies

Julianne J. Dalcanton<sup>1,2</sup>

Observatories of the Carnegie Institution of Washington, 813 Santa Barbara Street,  
Pasadena CA, 91101

&

Princeton University Observatory, Princeton, NJ 08544

David N. Spergel, & F J Summers<sup>3</sup>

Princeton University Observatory, Princeton, NJ 08544

## ABSTRACT

We present a scenario for the formation of disks which explains not only the properties of normal galaxies, but the properties of the population of low surface brightness galaxies (LSBs) as well. We use a gravitationally self-consistent model for disk collapse to calculate the observable properties of disk galaxies as a function of mass and angular momentum of the initial protogalaxy. The model naturally produces both smooth, asymptotically flat rotation curves and exponential surface brightness profiles over many disk scale lengths.

In this scenario, low mass and/or high angular momentum halos naturally form low baryonic surface density disks, which will tend to be low surface brightness. Theoretical and numerical calculations suggest galaxy halos should form with a wide range of mass and angular momenta, and thus, the disks which form within these halos should have a wide range of surface brightnesses and scale lengths. We use theoretical predictions for the distribution of halo masses and angular momenta to explicitly calculate the expected number density of disk galaxies as a function of central surface brightness and disk scale length. The resulting distribution is compared to the observed properties of galactic disks, and is shown to explain the range of observed disk properties, including the cutoff in the maximum disk scale length as a function of surface brightness. We also show that disk instabilities explain the observed lack of high surface density

---

<sup>1</sup>e-mail address: jd@ociw.edu

<sup>2</sup>Hubble Fellow

<sup>3</sup>Current Address: Columbia Astrophysics Lab, Mail Code 5247, 550 West 120th Street, New York, NY 10027

disks. The calculated distribution of disk properties also suggests that there are large numbers of galaxies which remain undetected due to biases against galaxies with either low surface brightness or small scale length. We quantify this by calculating the difference between the intrinsic luminosity function and the luminosity function which would be measured in a galaxy survey with a given limiting surface brightness. We show that current measurements of the galaxy luminosity function may be missing more than half of all  $L_*$  galaxies, and an even larger fraction of faint galaxies, given the correlation between mass and surface brightness. The likely underestimate of the luminosity density is also expected to be large. We discuss how this affects observations of the “faint blue galaxy” population.

We also investigate the dynamics of galaxies as a function of surface brightness. We show that, in the absence of any systematic change in the ratio of disk mass to disk luminosity, galaxies of all surface brightnesses should lie on the same Tully-Fisher (1977) relation. Our models also show systematic changes in the shape of the rotation curve as a function of angular momentum, which leads to low surface brightness galaxies having slowly rising rotation curves. Furthermore, because high angular momentum LSB disks have their baryonic mass spread over a larger area than normal galaxies of comparable mass, LSB disks contribute very little to the observed dynamics of the galaxy. Thus, LSBs provide a very effective tracer of the shape and mass profile of the dark matter halo, out to proportionally larger radii than is possible to observe with normal galaxy rotation curves.

## 1. Introduction

Disk galaxies, including low surface brightness galaxies (LSBs), show remarkable regularities: most disk galaxies have asymptotically flat rotation curves (see Bahcall and Casertano 1985, Burstein & Rubin 1985, Persic et al. 1995, de Blok et al. 1996, and the references therein); the Tully-Fisher relation between circular velocity and luminosity appears to hold over a wide range of both mass and surface brightness (Strauss and Willick 1995, Zwaan et al. 1995, Sprayberry 1995); and the light profile of galactic disks are well fit by an exponential over several disk scale lengths (de Jong 1995) for high surface brightness spirals, as well as for non-dwarf LSBs (Davies, Phillips, & Disney 1990, McGaugh & Bothun 1994, James 1994, McGaugh et al 1995, Dalcanton et al. 1997, DeJong 1995). The consistency of these properties suggests that the basic structure of all disk galaxies is a general property of galaxy formation, either tied to regulated feedback during formation, or,

as we shall consider in this paper, to primordial properties of protogalaxies, namely their mass and angular momentum. The fact that galaxies’ rotation curves are smooth in both the disk-dominated inner regions and the halo-dominated outer regions strongly suggests that the structure of the inner halo is coupled to the formation of the disk.

Past disk formation models have been able to reproduce many of the universal properties of disk galaxies (Fall & Efstathiou 1980, Gunn 1982, van der Kruit 1987). The models were motivated by Mestel’s (1963) observation that the angular momentum distribution of the galactic disk is very similar to that of a sphere in solid body rotation. Thus, the models assumed that the collapse of a uniformly rotating gaseous protogalaxy was a good model for the formation of the disk. In general, the models produced realistic disk surface density profiles, provided that the models included the further assumptions that 1) there was very little angular momentum transport while the gas is collapsing, 2) the angular momentum was responsible for eventually halting the collapse, and 3) the density profile of the dark matter halo was such that the resulting galaxy will have a flat rotation curve. However, because of the third assumption, the resulting mass distribution of the disk+halo system was not necessarily self consistent; because the halo did not respond to the mass of the collapsed disk, the final disk was not necessarily in gravitational equilibrium.

One limitation of past models of disk formation is that they have only attempted to reproduce the properties of “normal”, high surface brightness disks such as our own. However, a growing body of literature on low surface brightness galaxies (LSBs) has revealed that there is a substantial population of disk galaxies whose photometric properties fall well outside what is usually classified as “normal”. Any viable formation scenario must explain the tremendous range of disk galaxy surface brightnesses and scale lengths, while simultaneously explaining the tremendous similarities among disk galaxies throughout this range.

In this paper we develop a gravitationally self-consistent scenario for the formation of disks [§2]. It is remarkably effective at explaining both the structural and dynamical regularities among disks, as well as for motivating the enormous range of galaxy properties which are observed. We use the model to calculate directly observable properties of individual galaxies (light profiles [§2.1.1], rotation curves [§2.1.2], etc.). We also use it to compute the expected distribution of galaxies as a function of surface brightness and disk scale length; this allows us to easily calculate the degree to which selection effects shape the observed properties of galaxies [§3].

## 2. The Formation of Disks

The outline of the scenario which we will use for disk formation is as follows:

(1) In the early universe, tidal torquing spins up both the dark matter and the baryonic matter in some region of space, which we will approximate as an isolated sphere of radius  $a$  in solid body rotation (i.e. a rotating, spherical top-hat overdensity). While the region has enough of a mass overdensity that it will eventually collapse into a galaxy, the overdensity is small at early times ( $\delta \propto t^{2/3}$ ) and the mass density can be treated as uniform to first order. We also assume that the gas and the dark matter are uniformly mixed. Because inhomogeneities in the density field are sufficient to provide tidal torques (Peebles 1969), we do not require that large numbers of galaxies must have condensed before tidal torquing can be effective.

(2) As time passes, both the dark matter and baryonic matter begin to collapse in the overdense region. Initially, when the densities are low, the baryons cannot cool, and the pressureless collapse proceeds identically for both components.

(3) Because the dark matter cannot dissipate energy, its collapse halts when the system virializes. Numerical simulations suggest that the resulting halo has a generic density profile (Warren et al. 1992; Dubinski and Carlberg 1993; Navarro et al. 1996): inside the core radius, the density profile rises roughly as  $r^{-1}$ , while outside the core radius, the density profile falls as  $r^{-\gamma}$ , with  $\gamma$  between 3 and 4. We will approximate the halo with a Hernquist density profile, whose asymptotic radial profile scales as  $r^{-4}$  (see eqn 1 below). The size of the core radius depends only on the mass of the halo and the mean density of the universe. For a flat universe (which we will assume for simplicity for the duration of this paper), the growth of the halo is self-similar, and the only change in the halo with time is the increase in the core radius due to its increasing mass.

(4) At some point during the joint collapse of the dark matter and baryons, the density over some region becomes high enough that the baryons begin to cool and decouple from the dark matter. As they cool, their collapse accelerates, and the baryons begin to concentrate within the dark matter. This condensation progressively increases the baryonic fraction within the inner parts of the halo. Because the baryons have non-zero angular momentum they cannot collapse all the way to the center, and instead settle into a rapidly rotating disk. The final mass distribution in the disk is determined both by the initial distribution of specific angular momentum and by the final rotation curve of the collapsed disk+halo system.

(5) After the onset of cooling, the collapsing baryons further condense the dark matter halo by increasing the mass density in the inner parts of the halo, where the baryonic

mass fraction has increased the most. This modifies the Hernquist potential which the halo had at the time when cooling began. The condensation of the halo is assumed to proceed roughly adiabatically.

The calculation outlined above, which we perform explicitly in the following section, expands upon the formalisms of Fall & Efstathiou (1980), Gunn (1982), and van der Kruit (1987) by dropping the assumption of a static halo and allowing the disk halo to be pulled in by the collapsing baryons, while retaining the initial condition of a uniformly rotating protogalaxy and the assumption that the collapse time is much shorter than the angular momentum transport time.

An essential ingredient in our calculations is the assumption that angular momentum transport is negligible during the formation of disk galaxies. We have several reasons to believe that angular momentum transport is generally small, whether the formation is smooth, as we have assumed, or hierarchical, taking place through merging of low mass subunits. As we discuss at length in §3, the observed angular momenta of disks is comparable to what is expected for galaxy halos, suggesting that there has not been a dramatic drop in the angular momentum of the gas during formation. Furthermore, in numerical simulations within which the gas fails to conserve angular momentum during galaxy formation (e.g. Navarro & Steinmetz 1996), the disks which form are too compact and have too little angular momentum. In other words, angular momentum transfer between the gas and the dark matter halo leads to the formation of galaxies whose density profiles differ strongly from those of real galaxies. This empirical argument suggests that angular momentum transport between the gas and the halo is generally not important for the formation of disk galaxies.

Angular momentum transport during collapse is most likely to be negligible for the formation of low surface density disks, which as we shall show in §3, are the dominant form of disk galaxy; angular momentum transport is likely to be most effective in baryon-dominated systems such as ellipticals and bulges and least effective in low surface brightness systems. A pressure supported dark halo tends to suppress the formation of both bars (Ostriker and Peebles 1973) and spiral arms (Athanassoula 1984), two effective means of transporting angular momentum. In low surface density, high angular momentum systems, the dark matter dominates the potential, so bars and spiral arms are unlikely to form. On the other hand, in low angular momentum systems, dissipation concentrates the baryons to high densities, where they are subject to non-axisymmetric instabilities that will transport angular momentum. Thus, our basic assumptions are most likely to be valid for LSBs and are almost certainly not correct for ellipticals and the bulges of high surface brightness galaxies. Finally, we expect very little angular momentum transport within the

disk after its formation. The angular momentum transport time due to spiral density waves is quite long,  $\sim 5 - 10$  Gyr (Zhang 1996, Gnedin et al. 1995), and thus in the absence of bar formation or other large scale instabilities, disks cannot redistribute their angular momentum efficiently once formed.

The other major assumption about angular momentum is that the baryons have an initial angular momentum distribution similar to that of a uniformly rotating sphere. As in past disk formation models, our assumption is motivated by the similarity between the observed disk angular momentum distribution and the angular momentum distribution of a uniformly rotating sphere (Metsel 1963). Furthermore, in a simple picture of tidal torquing, most of the torqueing should occur near maximum expansion and will be due to an external quadrupole. This external torque will produce uniform rotation. Our assumption is also testable by comparison to numerical simulations, although current simulations have not addressed this problem explicitly.

Finally, in our model we appear to have assumed that all of the baryons collapse simultaneously, which is physically unreasonable. The baryons will begin to collapse beyond the dark matter when they begin to dissipate energy. The onset of cooling, however, is a density dependent phenomena, and the baryons in the densest, inner region of the halo will begin to collapse well before the outer region. However, because we are assuming that the system is spherically symmetric to first order, at any given time both the baryons and dark matter outside of the cooling region will be largely unaffected by how the matter inside the cooling region rearranges itself. Thus, while the arguments below are dependent on the initial and final distribution of the baryons, they are independent of the details of how the collapse proceeds to its final state, as long as the process is spherically symmetric and adiabatic.

## 2.1. Simple Model

In this section we will use the above scenario to calculate the mass profile of the disk and halo after collapse. The evolution of the mass profile can be traced through three distinct stages, each identified with a distinct length scale: 1) the uniform sphere before collapse, with radius  $a$ ; 2) the Hernquist profile with core radius  $r_0$ , at the moment when the majority of the baryons begin to decouple from the dark matter; and 3) the final baryonic disk, characterized by an exponential disk scale length  $\alpha$ . First we will use energy conservation to relate the core radius of the Hernquist profile halo to the radius of the initial protogalaxy. Next we will use adiabatic dragging of the halo and the initial angular momentum distribution of the disk to solve for the final mass profile and rotation curve

of the resulting galaxy. Finally, we will find the scale length, central surface brightness, and circular velocity of the resulting baryonic disk as a function of baryonic mass fraction, initial angular momentum, and the total galaxy mass.

The core radius  $r_0$  of the Hernquist profile can be easily related to the initial protogalaxy radius  $a$ , using energy conservation. Letting  $M_{tot}$  be the total mass within the initial sphere of radius  $a$ , and  $F$  be the fraction of mass within  $a$  which is baryonic, the potential energy of the dark matter in the initial sphere is  $-3(1-F)GM_{tot}^2/5a$ . This must be equal to the potential energy of the dark matter when the galaxy has partially collapsed into a Hernquist mass profile, defined as:

$$M_{halo}(r) = (1-F)M_\infty \left( \frac{r/r_0}{1+r/r_0} \right)^2 \quad (1)$$

where  $M_{halo}(r)$  is the halo mass within radius  $r$ . Its potential energy within a radius  $r$  is

$$\Phi \left( x \equiv 1 + \frac{r}{r_0} \right) = -\frac{(1-F)GM_\infty^2}{6r_0} \left[ 1 - \frac{6x^2 - 8x + 3}{x^4} \right]. \quad (2)$$

Fixing the mass within  $r = a$  to be constant,  $M_\infty = M_{tot}[(a+r_0)/a]^2$ . Assuming that the energy of the initial uniform sphere is entirely gravitational, that the energy of the halo within  $a$  is conserved during collapse, and that the energy of the collapsed Hernquist halo is roughly consistent with virialization ( $E \approx |\Phi|/2$ ), one finds that  $a = 3.2r_0$ . If virialization is not complete, the ratio of  $a/r_0$  will be somewhat smaller, but will not significantly change any of our results. The relationship between  $a$  and  $r_0$ , as well as all of the other relations derived in the section, are rederived in the Appendix for a shallower halo potential suggested by Navarro et al. (1996). With the shallower potential,  $a = 7.1r_0$ . For a flat universe, the evolution of a dark matter halo is a scale free process, thus, the density at the core radius should be a constant multiple of the mean density of the universe:  $r_0 = C^{-1}M_{tot}^{1/3}\rho_0^{-1/3}$ , where  $C \sim 70$  (Navarro et al. 1996) and  $\rho_0$  is the mean density of the universe. This allows the mass scale of the galaxy to be related to the initial size of the perturbation.

The next step is to calculate the mass distribution of the final disk, by considering the angular momentum distribution of the baryons and the adiabatic dragging of the dark matter by the collapsing disk. We have assumed that the baryons are evenly mixed with the dark matter before the onset of cooling, and that they have the distribution of specific angular momentum characteristic of disks today, which is well represented by a sphere in solid body rotation (Mestel 1963):

$$M_{gas}(< j) = FM_{tot} \left[ 1 - (1 - j/j_{max})^{3/2} \right], \quad (3)$$

where  $M_{gas}(< j)$  is the baryonic mass of the galaxy which has specific angular momentum less than  $j$ , and where  $j_{max} = \Omega a^2$  for a sphere in solid body rotation with angular rotation velocity  $\Omega$ . The maximum angular momentum can also be characterized by the spin angular momentum parameter  $\lambda \equiv J_{tot}|E|^{1/2}G^{-1}M^{-5/2}$  (Peebles 1969); for our initial conditions (i.e. an unvirialized sphere in solid body rotation)  $J_{tot} = 2M_{tot}j_{max}/5$  and  $E = -3GM_{tot}^2/5a$ , and therefore  $j_{max} = \frac{5}{2} \left( \frac{5}{3} \right)^{1/2} \lambda \sqrt{GM_{tot}a}$ .

We can now solve for the final mass distribution of the disk+halo system. To characterize the radial distribution of halo mass, we define  $m_h(r) \equiv M_{halo}(r)/(1 - F)M_{tot}$  to be the fraction of the halo mass enclosed within a radius  $r$ . We will use  $m_h$  as a radial parameter for the rest of this calculation, as well as a similar parameter related to the enclosed disk mass,  $m_d(r) \equiv M_{disk}(r)/FM_{tot}$ . (We will henceforth drop the explicit dependence of  $m_h$  and  $m_d$  upon  $r$  for notational convenience.) Note that the radial dependence of these parameters,  $r(m_h)$  (or  $r(m_d)$ ), will change during collapse, and thus while  $m_h$  always defines a surface bounding a certain fraction of the halo mass, the radius of that surface is not constant. After collapse, we will let  $M(m_h)$  ( $= M_{tot} [(1 - F)m_h + Fm_d(m_h)]$ ) be the total mass enclosed within  $r(m_h)$ .

Assuming that conservation of angular momentum is responsible for finally halting the collapse of the disk, the specific angular momentum of gas which halts at radius  $r(m_d)$  is  $j(m_d) = \sqrt{GM(m_d)r(m_d)}$ . All gas which has specific angular momentum less than  $j(m_d)$  will wind up interior to  $r(m_d)$ , and thus, using eq. 3,

$$m_d = \frac{M_{gas}(< j(m_d))}{FM_{tot}} \quad (4)$$

$$= 1 - \left( 1 - \frac{\sqrt{GM(m_d)r(m_d)}}{j_{max}} \right)^{3/2}. \quad (5)$$

Now, to calculate the final mass profile of the halo, the adiabatic invariance of the angular action  $I_\theta$  ( $\equiv \int \mathbf{v}_\theta \cdot r d\theta$ ) must be used (see Binney & Tremaine 1987, Chapter 3). Because the baryons collapse by a large factor, the time scale for their collapse is much larger than the orbital time of the dark matter at a given radius; therefore, the collapse is roughly adiabatic, and the orbits of dark matter particles will adjust to the changing potential such that  $I_\theta^2 = GM(r)r$  is constant (Blumenthal et al. 1985, Flores et

al. 1994). Using the inverted form of the Hernquist potential for the initial conditions,  $r_i(m_h) = r_0 m_h^{1/2} / (1 + r_0/a - m_h^{1/2})$ , after collapse the angular action is

$$GM(m_h)r(m_h) = Gm_h M_{tot} r_i(m_h) \quad (6)$$

$$= GM_{tot} r_0 \frac{m_h^{3/2}}{1 + (r_0/a) - m_h^{1/2}}. \quad (7)$$

Because  $M(m_h)r(m_h) = M(m_d(m_h))r(m_d(m_h))$ , eqn 6 may be substituted into eqn 5 to solve for  $m_d(m_h)$ , which then yields

$$m_d(m_h) = 1 - \left( 1 - \frac{\xi m_h^{3/4}}{\sqrt{1 + (r_0/a) - m_h^{1/2}}} \right)^{3/2}, \quad (8)$$

where  $\xi \equiv \sqrt{GM_{tot}r_0}/j_{max}$ , or  $\xi = 0.173/\lambda$ . Note that for small enough values of  $\lambda$ , there is some maximum  $m_h$  for which eqn. 8 is well defined; this cutoff corresponds to the maximum extent of the collapsed disk. For small values of lambda, the disk collapses to well inside the final extent of the halo, and beyond this extent,  $m_d$  should be fixed at 1.

The angular action may also be used to derive the final radius enclosing  $m_h$  of the halo mass:

$$r(m_h) = \frac{I_\theta(m_h)}{GM(m_h)} = r_0 \left( \frac{m_h^{3/2}}{1 + (r_0/a) - m_h^{1/2}} \right) \left( \frac{1}{(1 - F)m_h + Fm_d(m_h)} \right). \quad (9)$$

Coupled with

$$M(m_h) = M_{tot} [(1 - F)m_h + Fm_d(m_h)], \quad (10)$$

equations 8, 9, and 10 are parametric equations which fully specify the mass profile of the the collapsed galaxy. The final mass profile of the disk and halo therefore depends only on the baryonic mass fraction  $F$ , the density of the universe  $\rho_0$ , and the mass  $M_{tot}$  and spin angular momentum  $\lambda$  of the protogalaxy. Note that the only place where our choice of initial conditions (i.e. the uniform sphere) plays a significant role is in determining the numerical factor relating  $\xi$  to  $\lambda$ .

The above equations can be solved to give both the surface density and the rotation curve for the final disk:

$$\Sigma(r(m_h)) = \frac{FM_{tot}}{2\pi r(m_h)} \frac{dm_d}{dm_h} \frac{dm_h}{dr} \quad (11)$$

and  $v_c^2(r(m_h)) = GM(m_h)/r(m_h)$ .

As we will show in the following sections, for a  $10^{12}M_\odot$  halo with  $F = 0.05$  and  $\lambda = 0.06$ , the above model implies  $r_0 = 35\text{kpc}$ ,  $L = 1.7 \times 10^{10}L_\odot$ ,  $v_0 = 250 \text{ km/s}$ ,  $\alpha = 3.4 \text{ kpc}$ , and  $\mu_0 = 21.2 \text{ mag/arcsec}^2$ , all reasonable parameters for a massive disk galaxy (assuming a mass-to-light ratio of  $3 M_\odot / L_\odot$  for the baryons in the disk).

### 2.1.1. Surface Density

The calculations above solve for the mass of both the dark matter and the baryons as a function of radius, and thus they can be used to calculate the surface density profile of the baryonic disk which results from the collapse. Figures 1a and 1b show the disk surface density profile which results from eqn. 11 for different values of the dimensionless spin angular momentum  $\lambda$  and the galaxy mass  $M_{tot}$ . All of the disk profiles produced by this gravitationally self-consistent model are roughly exponential over many scale lengths, with a scale length  $\alpha$  that depends upon  $\lambda$ ,  $M_{tot}$ ,  $F$ , and  $r_0$ . After fitting the disk profile between 0.5 and 2.5 scale lengths for a wide range of parameters, we derive this approximate fitting formula for the scale length:

$$\alpha(M_{tot}, \lambda, F) \simeq 2.55r_0(M_{tot}) \left[ \frac{1}{2 + \lambda^{-1} + (0.084/\lambda)^2} \right]^{1+3F} [16F^2 + 8F + 1 + (0.002/F)]. \quad (12)$$

which is good to  $\pm 5\%$  over  $0.03 < \lambda < 0.18$ ,  $0.02 < F < 0.15$ , and  $1 \text{ kpc} < r_0 < 120 \text{ kpc}$ ; for larger values of  $\lambda$ , the formula overestimates the scale length by  $\sim 10\%$  at  $\lambda = 0.2$  and  $\sim 30\%$  at  $\lambda = 0.4$ . There is an apparent cut-off in the disks at large radii in Figure 1 which is due to using a sharp edged sphere in the initial conditions

Using the fact that the total disk mass is the baryonic fraction  $F$  times the total galaxy mass  $M_{tot}$ , the approximate central surface brightness is

$$\Sigma_0(M_{tot}, \lambda, F) = \frac{FM_{tot}}{2\pi\alpha(M_{tot}, \lambda, F)^2\Upsilon} \quad (13)$$

$$= \left[ \frac{\rho_0^{2/3} C^2}{13\pi\Upsilon} \right] \left[ \frac{F}{(1 + 8F + 16F^2 + \frac{0.002}{F})^2} \right] M_{tot}^{1/3} \left[ 2 + \lambda^{-1} + \left( \frac{0.083}{\lambda} \right)^2 \right]^{2+6F} \quad (14)$$

where  $\Upsilon = (M_{disk}/L_{disk})$ ; note that  $\Upsilon$  is not a dynamical mass-to-light ratio, but a measure of the efficiency of turning gas into starlight over the lifetime of the disk.

To first order,  $\Sigma_0 \propto FM_{tot}^{1/3} \lambda^{-(2+6F)}$ , suggesting that low mass and/or high angular momentum protogalaxies naturally form low surface brightness galaxies. Physically, because of angular momentum conservation, a more rapidly rotating protogalaxy will be unable to collapse as far inwards as a less rapidly rotating one. Thus, the galaxy with a larger specific angular momentum will spread its baryonic mass over a larger disk, leading to lower mass surface densities (as seen in eqns. 12 and 14). There is observational support for this picture from Zwaan et al. (1995) who find that LSBs have systematically larger scale lengths at a given circular velocity than their high surface brightness counterparts; given that the specific angular momentum must scale like  $\alpha V_c(\infty)$  to first order, LSBs must have higher angular momenta than normal galaxies of the same mass. Most importantly, Equation 14 also suggests that *any* spread in either the masses or the angular momenta of protogalaxies translates into a spread in the resulting distribution of disk surface densities. We will explore this effect in §3.

One feature of the models is the presence of a central cusp in the surface density distribution (Figure 1). The mass in the cusp is only a small fraction of the total disk mass ( $\sim 6\%$ ), and is largely independent of the choice of the initial mass profile of the halo (see Appendix A). The cusp is a consequence of our assumption that the angular momentum distribution is well-modelled by a uniformly rotating sphere (equation 3). The center of the disk contains the very low angular momentum material from the initial protogalaxy, and for a uniformly rotating sphere,  $M(< j) \propto j$  for  $j \ll j_{max}$ , implying  $\Sigma \propto r^{-1}$  in the central regions where the halo contributes very little to the total mass. In contrast, the surface brightness distribution of a pure exponential disk is constant for very small radii, and thus the surface brightness profiles that result from our models must necessarily be steeper than exponential in the center. Because the cusp is an artifact of our simple initial conditions, we do not ascribe any profound importance to the bulge-like centers of the model’s light profiles. Any variation in the shape of the initial perturbation, the alignment between the angular momentum and the principle axes of the perturbation, or the degree of angular momentum conservation will lead to variations in the size and shape of the cusp, and thus suggest natural mechanisms for producing variations in the bulge-to-disk ratio.

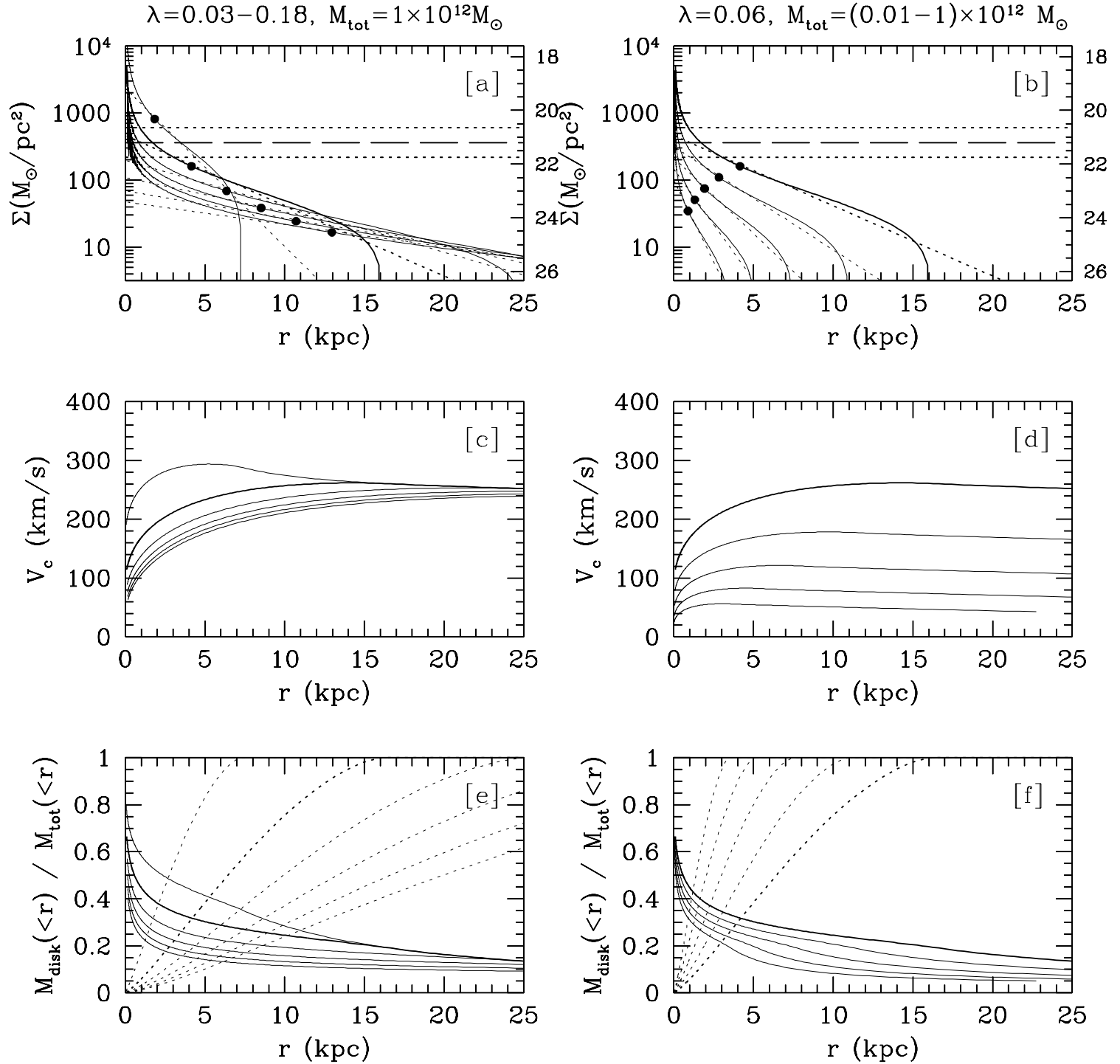


FIGURE 1  $\Rightarrow$

Fig. 1.—

Resulting surface density profiles [a,b], rotation curves [c,d], and disk mass profiles [e,f] for disk galaxy models with various angular momentum (left column;  $\lambda = 0.03 - 0.18$ , linearly spaced,  $M_{tot} = 10^{12} M_\odot$ ) and mass (right column;  $M_{tot} = 10^{10} - 10^{12} M_\odot$ , logarithmically spaced,  $\lambda = 0.06$ ). In all panels, the heavy line is a fiducial model with  $\lambda = 0.06$  and  $M_{tot} = 10^{12} M_\odot$ ; we have assumed  $F = 0.05$  and  $H_0 = 50 \text{ km/s/Mpc}$  for all the models. The top row [a-b] shows the surface density as a function of radius, with the right hand axis giving the apparent surface brightness  $\mu_0$  assuming a disk mass-to-light ratio of  $\Upsilon = 3 M_\odot/L_\odot$ . The horizontal dotted lines bracket the Freeman (1970) surface brightness. The solid lines are the models, the dotted diagonal lines are exponential fits to the surface brightness distribution, and the solid dots are at one exponential scale length ( $r = \alpha$ ). The models produce roughly exponential profiles over several scale lengths. Panel [a] shows how increasing the angular momentum of the protogalaxy decreases the extrapolated central surface brightness and increases the exponential scale length of the resulting disk, while panel [b] shows how increasing the mass of the protogalaxy increases both the central surface brightness and the scale length of the resulting disk. The middle row [c-d] shows the rotation curves which result from the models. Panel [c] shows that changing the angular momentum changes the shape of the rotation curve, such that high angular momentum models rise more slowly, but keeps the same asymptotic circular velocity. Panel [d] shows that decreasing the mass decreases the asymptotic circular velocity; the shape of the rotation curve does not change however, and simply rescales with the exponential scale length and mass. The bottom row [e-f] shows the baryonic-to-total mass fraction within a given radius (solid lines), as well as the fraction of the baryonic mass contained within a given radius (dotted lines). These plots show the degree to which the dynamics of the galaxy are strongly affected by the baryons. Panel [e] shows that in low angular momentum models ( $\lambda \leq 0.04$ ), almost all of the baryonic mass lies within a radius where baryons make up more than 40% of the total mass, whereas in high angular momentum models ( $\lambda \geq 0.09$ ), almost none of the baryonic mass falls in a region where baryons make up more than 40% of the total mass. The models also suggest that in the high angular momentum, low central surface brightness models, the halo dominates the dynamics over almost the entire disk. Panel [f] shows that for changing mass, the baryonic mass fraction is self-similar, scaling with the exponential scale length.

### 2.1.2. Rotation Curves

Equations 9 and 10 can readily be used to calculate the circular velocity as a function of radius. Figures 1c and 1d show the resulting rotation curves for the same disk plus halo models shown in Figures 1a and 1b respectively, for different values of the spin angular momentum  $\lambda$  and the total mass  $M_{tot}$ . For simplicity, we have included only the monopole term from the disk and not thus included the effects of disk flattening. The rotation curves confirm Blumenthal et al.’s (1985) and Flores et al.’s (1995) conclusion that adiabatic contraction of the halo leads naturally to asymptotically flat rotation curves, and, as previous authors have found, that for a wide range of parameters, the rotation curves of the models look much like those of real galaxies.

Figure 1[c&d] demonstrates how changes in mass and angular momentum affect the shape of the rotation curve  $V_c(r)$ . First, the shape of the rotation curve remains constant with changes in mass, when scaled by the exponential scale length, for fixed spin angular momentum  $\lambda$ . At fixed angular momentum, the baryons collapse by the same factor within the self-similar dark matter halos, leading to identical fractions of dark and luminous matter within a given dimensionless radius  $r/r_0$  (or  $r/\alpha$ ), and thus to self-similar rotation curves. However, if there is any deviation from perfect self-similarity in the shape of dark matter halos, then there will be accompanying deviations in the self-similarity of the rotation curves. Violations of our assumption of perfect self-similarity will lead to either increased scatter in the shape of rotation curves at fixed angular momentum, or to systematic variations in the shape of rotation curve with changing mass.

In contrast, changes in the spin angular momentum  $\lambda$  lead directly to variations in the shape of the rotation curve. Increasing the spin angular momentum of a galaxy decreases the collapse factor of the baryons (i.e.  $r_i/r_f$ ), leaving them at a larger dimensionless radius. Thus, an increase in the spin angular momentum reduces the fraction of baryonic mass within any given dimensionless radius, leading to a rotation curve whose shape is dominated more by the dark matter distribution than the baryonic matter. There are two strong observational signals of these high angular momentum rotation curves. First, high angular momentum galaxies will have a larger dynamical mass-to-light ratio, due to the increased dominance of dark matter over baryons at every radius (as can be seen in the mass profiles of Figure 1[e&f]). Second, the rotation curves will rise gradually with radius, instead of steeply as is usually observed for more concentrated low angular momentum disks.

As shown in §2.1.1, the models suggest that such high angular momentum systems should to be found preferentially among the population of low surface brightness galaxies (eqn 14). Indeed, the rotation curves of LSBs do reveal the same signatures as the high-angular momentum models. Edge-on (Goad & Roberts 1981) and face-on LSBs (de

Blok et al 1996) show a systematically slower rise in their rotation curves than do their high surface brightness counterparts. De Blok et al (1996) also find that the dynamical mass-to-light ratio increases systematically with surface brightness, in concordance with the model.

The rotation curves in Figure 1[c&d] and the mass profiles in Figure 1[e&f], suggest that low surface brightness disks are extremely good tracers of the properties of dark matter halos. First, because low surface density disks contribute less to the dynamics of the galaxy within any given radius, the resulting rotation curve is much closer to what would be expected for a massless disk. Second, LSB disks will tend to reflect any deviations from axisymmetry within the halo. Because the disks do not have enough mass to round out the potential at a given radius, the disks should be more asymmetric in general; however, if LSBs are high angular momentum systems, they may preferentially form in halos with large quadrupole moments, which will lead to a further increase in the apparent disk asymmetry. Finally, LSBs have larger scale lengths than high surface brightness galaxies of the same mass. This allows the halo to be traced to a much larger radius, allowing the mass profile of the halo to be measured at extremely large distances.

We may make a detailed comparison between the shapes of observed rotation curves and the rotation curves produced by the models. Figure 2 shows the  $\log R$ - $\log M(R)$  relations for the Burstein & Rubin (1985) “mass types” (derived from observed rotation curves) and the identical relation for models spanning a moderate range of spin angular momenta. (All of the curves have been rescaled by an arbitrary factor  $R_m$  and  $M_m$  to match at their point of maximum inflection (as in Burstein & Rubin 1985), and the model curves have been shifted upwards from the observations to make the comparison easier.) Figure 2 shows that, one, both the models and the observations are remarkably similar, with the rotation curves being well approximated a broken power-law, and two, that it is the faster rising rotation curves which have less curvature. In the models, these changes in shape are produced by reasonable variations in the spin angular momentum. Furthermore, because changes in mass do *not* produce changes in the shape of the rotation curve, there should not be any strong correlation between galaxy mass and the distribution of Burstein & Rubin “mass types”, unless the dark matter halos are not self-similar with mass, as we have assumed. There is a tendency for the model mass distributions to be slightly shallower at small radii than the observed distributions, which probably reflects either a deviation from the assumed initial Hernquist halo mass profile or in the initial distribution of angular momentum. Given the simplicity of the initial assumptions, this is less notable than the general degree of agreement.

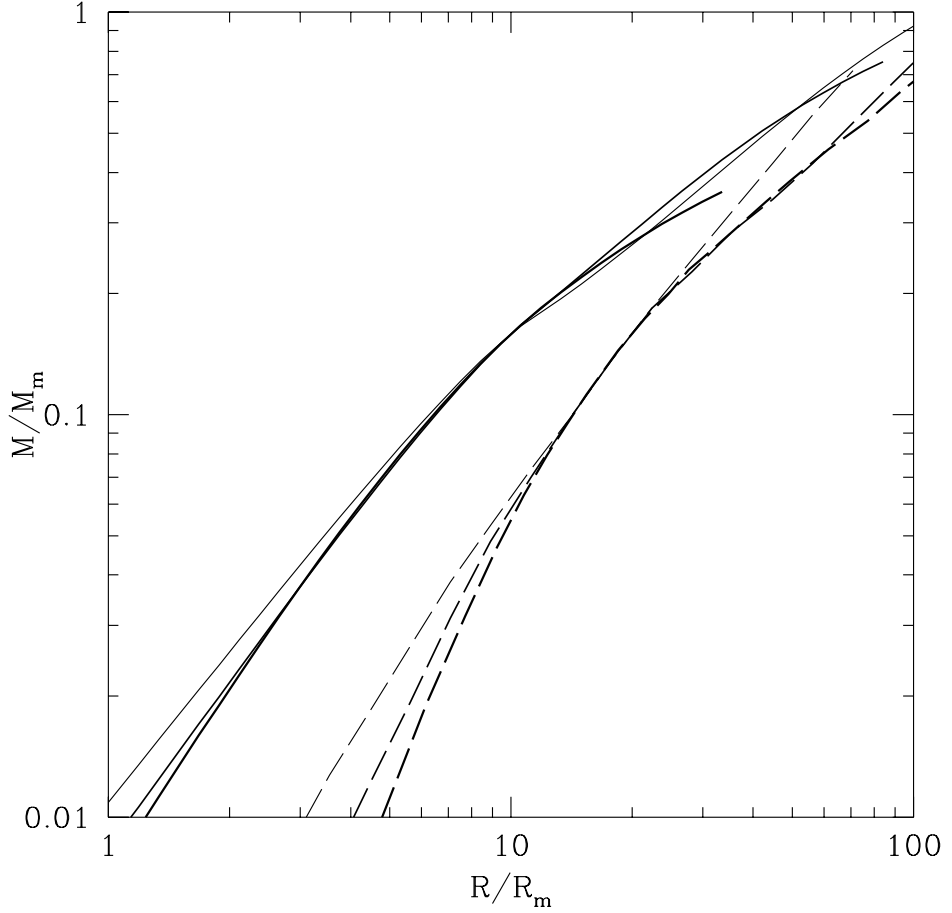


Fig. 2.— Comparison between the shapes of the rotation curves resulting from models with  $\lambda = 0.03$  (light solid),  $\lambda = 0.05$  (medium solid), and  $\lambda = 0.03$  (heavy solid), and the Burstein & Rubin (1985) “mass types” I (light dashed), II (medium dashed), and III (heavy dashed). The curves have been rescaled in radius and mass to match at their points of maximum curvature, as in Burstein & Rubin (1985). Changes in angular momentum are clearly capable of producing variations in shape comparable to those found observationally by Burstein & Rubin. The models rise less steeply in the center and more slowly in the outer regions than do the Burstein & Rubin mass types. This probably reflects a difference between reality and our assumed halo profile or angular momentum distribution, as well as possibly our neglect of bulges.

Recent work by Persic, Salucci, & Stel (1996; see also Persic & Salucci 1996) has parameterized the shape of galaxy rotation curves as a function of mass to produce a “Universal Rotation Curve” (URC). However, as our modelling shows, such attempts may perhaps reveal more about the selection criteria of the sample of galaxies used to generate the URC than about the rotation curves themselves. First, because mass and angular momentum are fundamentally linked with surface brightness and exponential scale length, any selection bias which affects the distribution of surface brightnesses and scale lengths present in a galaxy sample will critically affect any URC derived from the sample; any selection effect which changes the distribution of surface brightnesses and scale lengths in a sample can change the apparent distribution of disk angular momenta, and thus the distribution of rotation curve shapes. For example, intrinsically large scale lengths will be overrepresented in angular diameter limited surveys of field galaxies, while an angular diameter limited surveys of cluster galaxies will have a larger fraction of galaxies with small scale lengths. Thus the two surveys will have different distributions of galaxy masses and angular momenta, giving different apparent relations between mass and rotation curve shape. Furthermore, there are unavoidable biases against finding low surface brightness galaxies, which will tend to reduce the contribution of low mass or high angular momentum galaxies to the derived URC. To avoid drawing any erroneous conclusions, any parameterization of rotation curve shapes must include a detailed discussion of the selection criteria that went into choosing the galaxies whose rotation curves were measured.

### 2.1.3. *Tully-Fisher Relation*

In addition to understanding the shape of galaxy rotation curves, our models may be used to understand the behavior of the Tully-Fisher relation as a function of surface brightness. Towards that end, fitting the circular velocity at three disk scale lengths, we find

$$V_c(r = 3\alpha; r_0, \lambda, F) = 8 \text{ km/s} \left[ \frac{r_0(M_{tot})}{\text{kpc}} \right] [a(\lambda)F + b(\lambda)] \quad (15)$$

where

$$a(\lambda) = 1 + 35 \left[ \frac{(0.015/\lambda)^2}{1 + (0.015/\lambda)^2} \right] \quad (16)$$

and

$$b(\lambda) = 0.22 + 0.68 \left[ \frac{(\lambda/0.015)}{1 + (\lambda/0.015)} \right], \quad (17)$$

which is accurate to  $\pm 5\%$  for  $0.01 < \lambda < 0.14$ ,  $0.01 < F < 0.15$ , and  $1 \text{ kpc} < r_0 < 120 \text{ kpc}$ . The lambda dependence (i.e. the term in brackets) in equation 15 contributes only a  $\pm 20\%$  variation in  $V_c$  for  $\lambda > 0.025$ . For very small angular momentum models, however, the concentration of the disk is substantial enough that the mass of the compact disk contributes significantly to the rotation curve, giving a factor of two variation in  $V_c$  for  $\lambda < 0.025$ . However, these systems are the least likely to survive as pure disk galaxies; these low angular momentum disks are disk dominated in their centers and are likely to be unstable to bar formation. The bar would transfer angular momentum outwards to the halo (Weinberg and Hernquist 1992), which redistributes angular momentum within the galaxy and alters its structure. The low angular momentum systems are also plausible candidates for elliptical galaxies.

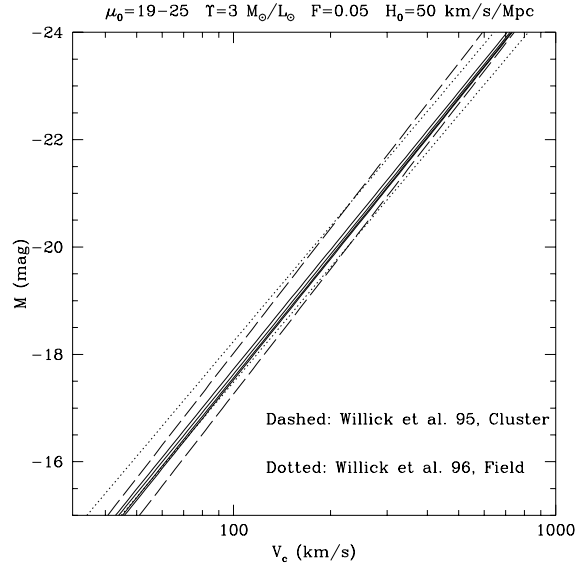


Fig. 3.—

Comparison between the Tully-Fisher relation predicted by equation 15 for  $\mu_0 = 19 - 25 \text{ mag/arcsec}^2$  (solid lines, lighter corresponding to fainter surface brightness) and the observed Tully-Fisher relation ( $\pm 1\sigma$ ) for clusters (dashed line; Willick et al. 95) and the field (dotted line; Willick et al. 96). Note that, for the assumption of a constant mass-to-light ratio for galactic disks, there should be no shift in the mean Tully-Fisher relation as a function of surface brightness. We have assumed  $\Upsilon = 3 M_\odot/L_\odot$ ,  $F = 0.05$ , and  $H_0 = 50 \text{ km/s/Mpc}$  for the models.

Equation 15 above can be used to understand the Tully-Fisher relationship (Tully & Fisher 1977; see Strauss & Willick 1995 for a review) for disk galaxies, for *all* surface brightnesses. Because the scale length of the disk is proportional to  $r_0$  (eqn. 12), and the circular velocity at fixed scale length is proportional to  $\sqrt{M(r)/r_0}$ , giving  $L \propto V_c^3$ , with a numerical constant that depends upon  $F$ ,  $\Upsilon$ , and  $\lambda$ . This slope is consistent with the observed infrared Tully-Fisher relation (Strauss and Willick 1995). Furthermore, because of the weak dependence of  $V_c$  upon  $\lambda$ , equation 15 predicts very little offset in the Tully-Fisher relation with changes in  $\lambda$ , and thus predicts that the Tully-Fisher relations for both high and low surface brightness galaxies should be nearly coincident. We show this in Figure 3, where we plot the relationship between circular velocity and absolute magnitude predicted by equation 15 for a wide range of disk surface brightnesses. Superimposed are the  $\pm 1\sigma$  limits for the Tully-Fisher relation derived by Willick et al (1995, 1996) for normal cluster and field galaxies. The predicted Tully-Fisher relations fall well within the observed scatter over a factor of 100 in surface brightness and a factor of 1000 in mass.

The independence of the predicted Tully-Fisher relation and disk surface density is not surprising given that the relation primarily results from the properties of the dark matter halo, if one reasonably assumes that the luminosity of a galaxy is proportional to the total mass, and that the measured line width reflects the asymptotic circular velocity at large radii, where the mass is dominated by the halo; the relationship between luminosity and line width should not depend strongly on how the baryons are distributed within the halo. However, the predicted relations do assume a single disk mass-to-light ratio  $\Upsilon$  for all masses and all disk surface densities; any variation in  $\Upsilon$  should translate into increased scatter in the relation, and any systematic variation in  $\Upsilon$  with the total mass or surface density of the disk should translate into changes in the Tully-Fisher slope. Therefore, the remarkable agreement between the predicted Tully-Fisher relation in Figure 3 and the measured one implies that there is very little evidence for a systematic variation of the disk mass-to-light ratio with mass. On the other hand, while Sprayberry et al. (1995) and Zwaan et al. (1995) both find that LSB galaxies fall on the same Tully-Fisher relation defined by normal galaxies, they also find increased scatter in the relationship, roughly by factors of two. This suggests that there is more variation in the disk mass-to-light ratio for low surface density disks than for high surface density disks; given the more tenuous nature of these disks, we do not find this conclusion to be unreasonable. However, given that the mean Tully-Fisher relation is indistinguishable for both high and low surface brightness galaxies, the mean disk mass-to-light ratio must be similar across the range of observed surface brightnesses.

## 2.2. Pressure Support

In the preceding calculation of the galaxy formation, we assumed that the baryons will collapse along with the dark matter halos. However the baryonic gas experiences pressure forces in addition to gravitational forces. For small masses, internal pressure may support the gas against collapse, in spite of the inward gravitational pull of the collapsed dark matter halo (Jeans 1929). Because of the link between low masses and low surface brightnesses (eqn 14), there is some limiting surface density for which we expect our assumption of complete baryonic collapse to become invalid.

To constrain the regime of galaxy properties for which pressure support can affect the formation of a disk, we consider the simpler question: what is the range of halo properties for which the gas is bound to the dark matter halo? The gas will be bound if the gravitational binding energy is greater than its thermal energy. Assuming that the gas is fully ionized, it will be gravitationally bound to the dark halo if

$$\frac{m_p V_c^2}{2} > kT, \quad (18)$$

where  $V_c$  is the circular velocity of the dark matter halo,  $m_p$  is the proton mass, and  $T$  is the temperature of the gas. Applying this relation at the halo half mass radius, where  $v_c = \sqrt{GM/r_0} = \sqrt{GCM^{1/3}\rho_0^{-1/6}}$  implies a minimum halo mass for collapsed objects:

$$M_{\min} = \rho_0 \left( \frac{kT}{G\rho_0 m_p C} \right)^{3/2} = 4 \times 10^7 M_\odot T_4^{3/2} \quad (19)$$

where  $T_4 = T/10^4 K$ . Thus, the Jeans criterion limits the formation of low mass galaxies, rather than low surface brightness galaxies, and we can treat the above calculation as valid for all protogalaxies with  $M_{tot} > M_{\min}$ .

## 3. The Number Density of Disk Galaxies

The equations of §2.1.1 provide a means to relate the primordial quantities of mass and angular momentum to the observable properties of disk galaxies, namely central surface brightness and scale length. Theoretical models and numerical simulations provide a way to predict the distribution of mass and angular momentum for galaxy halos, and thus we have the means to predict the observed distribution of disk central surface brightnesses ( $\mu_0$ ) and scale lengths ( $\alpha$ ). Furthermore, because most selection effects in galaxy catalogs can

be modelled as detection efficiencies as a function of surface brightness and/or scale length, the resulting joint distribution of  $\mu_0$  and  $\alpha$  can be convolved with a model of a survey’s detection efficiency to predict the observed distribution of either  $\mu_0$  and  $\alpha$ , or equivalently, surface brightness and luminosity.

To begin, we must first assume an intrinsic distribution for spin angular momenta,  $p(\lambda)$ . This problem has been approached both analytically and numerically by a number of groups (Barnes & Efstathiou 1987, Ryden 1988, Warren et al. 1992, Eisenstein & Loeb 1995, Catelan & Theuns 1996a, Catelan & Theuns 1996b), all of which find the same general properties. To first order, the distribution of spin angular momentum of collapsed dark matter halos is well approximated by a log normal distribution:

$$p(\lambda) = \frac{1}{\sigma_\lambda \sqrt{2\pi}} \exp\left(-\frac{\ln^2(\lambda/\langle\lambda\rangle)}{2\sigma_\lambda^2}\right) \frac{d\lambda}{\lambda}. \quad (20)$$

Most work finds that this distribution peaks around  $\langle\lambda\rangle \approx 0.05$ , with a width in the log of  $\sigma_\lambda \simeq 1$ . For the purposes of this paper, we adopt the specific values of  $\sigma_\lambda \simeq 0.7$ , and  $\langle\lambda\rangle \simeq 0.06$ , which provide a good fit to the results of Warren et al. (1992).

For simplicity, we will assume that  $p(\lambda)$  is identical for all sizes of the initial density perturbation (i.e. angular momentum is independent of mass). Faber (1982) has argued that the spin angular momentum of a protogalaxy should be independent of the amplitude of the initial overdensity, based upon scaling laws. However, there is some evidence from analytic calculations of  $p(\lambda)$  in the peak-height formalism which suggests that the mean spin angular momentum,  $\langle\lambda\rangle$ , is a function of the height of the peak in the initial density field which forms a given protogalaxy (Eisenstein & Loeb 1995, Catelan & Theuns 1996a): The trend is such that smaller initial peaks, which are likely to be more asymmetric, are more subject to torques and have larger mean angular momenta; this would make it even more likely to find that low mass galaxies are also low surface brightness galaxies, and could potentially lead to systematic variations in galaxy-galaxy correlation properties as a function of surface brightness. However, given that the shift in angular momentum distribution with peak height has yet to be verified numerically, we will retain the simple assumption of the independence of angular momentum and peak height.

Another of our assumptions is that the angular momentum of the gas is conserved during collapse, independent of the parameters of the collapse. This assumption should be robust when a collapse can be approximated as smooth; for example, in a collapse where there are no major mergers, or where the gas in merging subclumps is extended and hot enough that there is little angular momentum transfer between the gas clumps and the dark matter halos. However, the degree to which angular momentum conservation holds may

well depend on the detailed merger history of a given galaxy, which in turn could depend systematically on mass, angular momentum, and peak height.

While there are theoretical and numerical tools for approximating the merger history of galaxy halos of a given size (e.g. Bower 1991, Bond 1991, Lacey & Cole 1993, 1994), there is not a consistent picture of the behavior of gas in these merging systems which leads to the observed galaxy structure. For example, depending on the assumptions about the ultraviolet background radiation and star formation feedback, galaxies in hierarchical formation scenarios can have from 30% to 90% of their gas cool (Navarro & White 1993, Evrard, Summers, & Davis 1994, Thoul & Weinberg 1996, Navarro & Steinmetz 1996). A consistent feature is that these simulations produce disks in which the gas is much more centrally concentrated than in disks of real spiral galaxies. The spin parameters of the simulated disks show a range of values, generally below those observed, and indicate some angular momentum transport to the dark matter. However, given the developing nature of the field and, more importantly, the failure to reproduce the observed gas profiles, it would be imprudent to assume angular momentum transport plays a strong role in galaxy formation and we have no firm basis for considering its variation with the properties of galaxy halos.

In principle, any modification can be worked into equation 20, but, for now, we take the properties of the dark matter halos as representative of the properties of the resulting disks. This simplification may eventually prove to be a poor assumption for some individual galaxies, but it would be incorrect in general only if there were such extensive, violent merging as to entirely erase any memory of the initial angular momentum distribution from the resulting gas distributions, for the bulk of the galaxy population. Such a scenario seems unlikely as it raises serious questions about why spiral galaxies have angular momenta which are comparable to the predicted angular momenta of dark matter halos and how one avoids excessive central gas concentrations in such a model.

In addition to the above distribution of spin angular momenta, to fully specify the predicted distribution of disk central surface brightnesses and scale lengths we also need a prediction for the distribution of galaxy masses. As a first approximation, we use a Schechter function with a power law of slope  $\alpha$  at the low mass end, with an exponential cutoff at masses greater than  $M_*$ , such that

$$n(M_{tot}) = \Phi_* (M_{tot}/M_*)^{\alpha_{lum}} \exp(-M_{tot}/M_*). \quad (21)$$

(Press & Schechter 1974, Schechter 1975).

With the above distribution of spin angular momenta and galaxy masses, we may calculate the predicted distribution of disk central surface brightnesses and scale lengths.

First, we may use the distribution of angular momentum in equation 20 and the relationship between surface brightness and angular momentum in equation 14 to calculate the predicted distribution of disk surface brightness at fixed disk mass:

$$p(\Sigma_0|M_d) = p(\lambda) \left| \frac{d\lambda}{d\Sigma_0} \right|_{M_d}, \quad (22)$$

which requires the following inversion of equation 14:

$$\lambda(\Sigma_0|M_d) = \frac{A + \sqrt{0.944A^2 + 0.028A}}{2 - 4A}, \quad (23)$$

where

$$A = \left[ \frac{\sqrt{M_d/2\pi\Upsilon\Sigma_0}}{2.55r_0(1 + 8F + 16F^2 + \frac{0.002}{F})} \right]^{\frac{1}{1+3F}}. \quad (24)$$

Then, with equations 12 and 22 and the distribution of galaxy masses  $n(M_d)$ , the joint distribution of central surface brightness and scale length is

$$\begin{aligned} n(\alpha, \Sigma_0) &= n(M_d, \Sigma_0) \left| \frac{dM_d}{d\alpha} \right| \\ &= p(\Sigma_0|M_d) n(M_d(\Sigma_0, \alpha)) \left| \frac{dM_d}{d\alpha} \right|. \end{aligned} \quad (25)$$

All of the above equations involving the central surface brightness  $\Sigma_0$  can easily be reformulated in terms of magnitude per square arcsecond,  $\mu_0$ , using the conversion  $p(\mu) = p(\Sigma_0)\Sigma_0/(2.5 \log e)$ .

Because the distribution of angular momenta (eqn. 20) is broad, spanning more than a factor of 10 in  $\lambda$ , equations 14 and 22 suggest that the distribution of galaxy surface brightnesses should also be broad<sup>4</sup>. For example, keeping only the  $\lambda^{-2-6F}$  dependence of equation 14, the log-normal distribution of angular momenta (eqn. 20) leads to a Gaussian

---

<sup>4</sup>Note that van der Kruit (1987) came to a nearly opposite conclusion with a similar analysis, by assuming that disk galaxies had one unique value of  $\lambda$ . His Equation 15 (an analog to our equation 13) therefore predicted a single characteristic disk surface density.

distribution of central surface brightness  $\mu_0$ , with width  $\sigma_\mu = 2.5(2 + 6F) \log(e)\sigma_\lambda$ , or roughly  $2.5\sigma_\lambda \text{ mag/arcsec}^2$ . Given that most numerical studies find  $\sigma_\lambda \sim 0.7$ , there is immediately reason to expect galactic disks to form with a very wide distribution of central surface brightnesses, at every luminosity.

The peak of the (approximately) Gaussian surface brightness distribution corresponds to a characteristic surface brightness for each given mass:

$$\begin{aligned}\langle\mu_0\rangle &= 27.07 - 2.5 \lg \left( \frac{\rho_0^{2/3} C^2}{13\pi\Upsilon} \right) \left[ \frac{F}{(1 + 8F + 16F^2 + \frac{0.002}{F})^2} \right] M_{tot}^{1/3} / \langle\lambda\rangle^{2+6F} \\ &= 22.7 + 2.5 \lg \frac{\Upsilon}{3 M_\odot / L_\odot} - 0.83 \lg \left[ \frac{M_d}{10^{10} M_\odot} \right],\end{aligned}\quad (26)$$

in units of  $B$  magnitudes per square arcsecond, assuming  $F = 0.05$ . The characteristic surface brightness for “normal” bright galaxies is therefore comparable to the canonical Freeman (1970) value of  $21.7 \pm 0.3 \text{ mag/arcsec}^2$  for disks. However, the expected width of  $\pm 3.4$  magnitudes suggests that there will be large numbers of bright galaxies with very faint disk surface brightnesses, down to  $\sim 24 \text{ mag/arcsec}^2$ ; at lower luminosities, the expected distribution of disk properties will shift to even lower surface brightnesses.

### 3.1. The Distribution of Surface Brightness and Scale Length

The general picture that the above sections describe is one where the structure of galaxy disks can be directly linked to mass and angular momentum through equations 12 and 14. At fixed angular momentum, low mass galaxies have faint central surface brightnesses and small scale lengths. At a fixed mass, galaxies with large angular momentum spread their mass over a larger area, leading to large scale lengths but faint central surface brightnesses. Therefore, we expect to find galaxies with a wide range of surface brightnesses and scale lengths, due to variations in mass and angular momenta among protogalaxies. We may take the distribution of surface brightness and scale length predicted by this scenario (eqn. 25) and compare it with the observed properties of the population of disk galaxies.

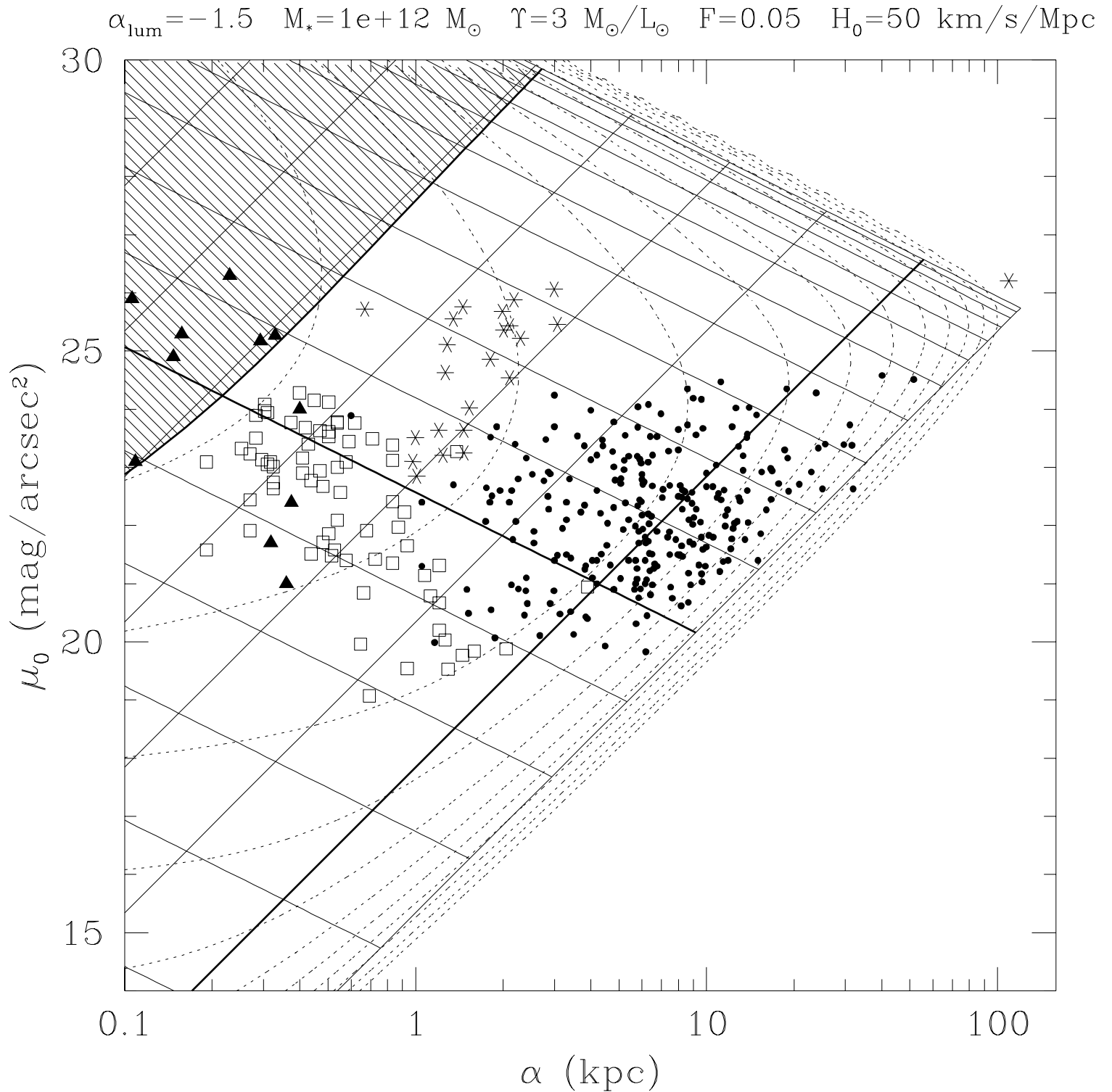


FIGURE 4  $\Rightarrow$

Fig. 4.—

Observed and predicted distribution of exponential scale lengths  $\alpha$  and central surface brightness  $\mu_0$  (in the  $B$  band) for galactic disks. The solid circles are taken from a variety of sources (Romanishin et al. 1973, Boroson 1981, van der Kruit 1987, Sprayberry et al. 1995, de Blok et al. 1995, McGaugh & Bothun 1994, de Jong & van der Kruit 1994, de Jong 1996, Knezeck 1993), and consist mostly of galaxies chosen from the NGC, the UGC, or the POSS-II catalog of LSBs (Schombert et al. 1992), all of which are either explicitly or implicitly angular diameter limited field surveys; however, because of how the points were assembled from the literature, the filled circles cannot be used to determine the relative number densities of galaxies as a function of  $\alpha$  and  $\mu_0$ , although they do give a good indication of the range of galaxy properties found in field surveys. The open squares are from the center of the Virgo cluster (Bingelli et al. 1984), the stars are from a catalog of LSBs in the direction of the Virgo cluster (Impey et al. 1988), including Malin I (upper far right). The filled triangles are the local group dwarf spheroidals compiled by Caldwell et al. 1992. The dotted lines are contours of constant  $n(\lg \alpha, \mu_0)$  (from equation 25), assuming  $\Upsilon = 3 M_\odot/L_\odot$ ,  $F = 0.05$ , and  $H_0 = 50 \text{ km/s/Mpc}$  (which are the same parameters which fit the Tully-Fisher relation in Figure 3), and assuming  $\alpha_{lum} = -1.5$ ,  $M_* = 10^{12} M_\odot$ ,  $\langle \lambda \rangle = 0.06$ , and  $\sigma_\lambda = 0.7$  for the mass and angular momentum distributions. The diagonal solid lines of positive slope are lines of constant mass (separated by factors of 10, with the heavier line at the characteristic mass  $M_*$ ), and the diagonal solid lines of negative slope are lines of constant angular momentum (logarithmically spaced, separated by factors of  $10^{0.2}$ , with the heavier line at a characteristic angular momentum  $\lambda > \sim 0.06$ ). The cross-hatched region in the upper left corner is the area where gas pressure will prevent galaxies from collapsing (i.e.  $M < M_{min}$ ; §2.2). Note that: 1) the region of the plane occupied by galaxies is strongly dependent on the type of survey used to find the galaxies; 2) cluster surveys, which are largely unbiased with regard to physical scale length, are dominated by galaxies with low surface brightnesses and small scale lengths, as would be predicted by  $n(\lg \alpha, \mu_0)$ ; 3) both the data and the models show the same paucity of physically large, high surface brightness galaxies, which reflects the exponential mass cutoff in the mass function of galaxies; and 4) galaxies exist with the lowest surface brightnesses to which the deepest surveys are sensitive, suggesting there are likely to be galaxies with even lower surface brightnesses than have currently been observed. See §3.1 for a fuller discussion.

In Figure 4, the distribution of surface brightness and scale length predicted by equation 25,  $n(\lg \alpha, \mu_0)$ , is drawn as dotted contours separated by factors of 10 in number density. Superimposed upon these contours are diagonal lines of constant disk mass (the solid lines of positive slope) and lines of constant angular momentum (the solid lines of negative slope). The distribution plotted in Figure 4 shows several observationally testable features. First, the distribution is extremely broad in both surface brightness and scale length, suggesting that disk galaxies should form with an extremely wide range of properties. Second, looking at  $n(\lg \alpha, \mu_0)$  along a line of constant mass, the distribution suggests that galaxies of any mass have a wide range of surface brightnesses. Thus, low surface brightness galaxies are not necessarily dwarf galaxies, and many examples should be found with masses which are comparable to normal galaxies. Third, both normal and low surface brightness galaxies should show the exponential cutoff with mass. At the cutoff, low surface brightness galaxies will have systematically larger scale lengths due to their high angular momentum. These effects lead to an apparently larger maximum disk scale lengths with decreasing surface brightness (i.e. the diagonal edge in Figure 4 towards high surface brightness and large scale length). Fourth, the number density rises with decreasing scale length and decreasing surface brightness, suggesting that there is an enormous population of small, low surface brightness galaxies. The rise is due to a combination of the increase in the galaxy mass function with decreasing mass, and of the correlation between mass and surface brightness and/or scale length (eqns 13 & 12). Finally, Figure 4 suggests that there should be a correlation between mass and surface brightness. The correlation results from eqn 13, which suggests surface brightness is proportional to  $M^{1/3}$ . However, as can be seen by the contours of  $n(\lg \alpha, \mu_0)$ , the correlation will be broad, due to the width of the angular momentum distribution. The correlation may be the source of the surface brightness - luminosity relation found by Bingelli et al. (1984) in the Virgo cluster, and by Ferguson & Sandage in Fornax (1988).

To compare the predicted distribution of  $n(\lg \alpha, \mu_0)$  to observations of disk galaxies, in Figure 4 we have also plotted observed properties of galactic disks for a variety of surveys with different selection techniques. Because selection effects are largely responsible for shaping the apparent distribution, for the moment we will restrict our comparison to galaxies discovered exclusively in large photographic angular diameter limited field surveys (i.e. NGC, UGC (Nilson 1973), POSS-II LSB survey (Schombert et al. 1992), APM LSB survey (Impey et al. 1996)), all of which have similar angular diameter limits and thus similar selection criteria. These field galaxies are plotted as filled circles in Figure 4, based upon their published surface brightness photometry. While little can be said about the relative number density of the field galaxies on this plot, given that the disk properties are drawn from a variety sources, there are some clear trends in the range of observed disk

properties. First, there is an apparent cutoff at faint surface brightness, which reflects selection biases against LSBs; the lowest surface brightness galaxies among the filled circles are barely visible on the photographic plates used for discovery<sup>5</sup>. Second, there is an apparent cutoff at small exponential scale lengths. The cutoff results from selection biases in angular diameter limited surveys from which the galaxies were drawn. Angular diameter limited surveys are heavily biased towards finding galaxies with the largest scale lengths and against finding intrinsically small galaxies; unless it is incredibly close, a very small galaxy will not have a large enough angular extent to be included in the survey. Therefore, physically large galaxies will be strongly over-represented in angular diameter limited surveys.

There are two other boundaries in the observed distribution of disk properties in Figure 4 which are physically meaningful, and are not due to selection biases. First, there is an apparent absence of large, high surface brightness galaxies, as can be seen from the diagonal cutoff in the lower right. This cannot be due to selection effects, given that these galaxies are the easiest of all possible galaxies to detect. However, this cutoff agrees well with the cutoff in the predicted distribution of scale lengths and surface brightnesses, calculated above and plotted as the dotted contours.

The second physically important cutoff in the distribution of disk properties is the absence of high surface brightness galaxies. Equation 26 and Figure 4 suggest that there will be significant numbers of galaxies which have surface brightnesses brighter than the Freeman surface brightness (1970). However, while there are many galaxies with surface brightnesses *fainter* than the Freeman value, there are *no* galaxies observed with surface brightness much brighter than the Freeman value (Allen & Shu 1979).

In Figure 4 there is a maximum surface brightness at roughly  $\mu_0 = 19.5 \text{ mag/arcsec}^2$ , above which galaxy disks do not seem to form. We postulate that these galaxies either lose substantial amounts of angular momentum during collapse or become unstable to global modes after formation; both processes would cause the disk to lose both energy and angular momentum, leading to the formation of bulges and/or ellipticals. Support for this idea comes from a stability analysis of our model disks using the Toomre criteria for the stability of a rotating stellar disk ( $Q \equiv \frac{\sigma_{V_r} \kappa}{3.36 G \Sigma} > 1$  for stability (Toomre 1964), where  $\sigma_{V_r}$  is the radial velocity dispersion of the stars, and  $\kappa$  is the epicyclic frequency). While the Toomre criteria is derived for local disk stability, it gives a reasonable prediction of a disk's

---

<sup>5</sup>Note that historically only galaxies with  $\mu_0 \lesssim 22 \text{ mag/arcsec}^2$  have been well studied due to their easy detectability. While this surface brightness regime spans a reasonable range in mass, it only covers a limited range in angular momentum, leading to the (false) impression that, not only do disks have a characteristic surface brightness, they have a characteristic angular momentum as well.

stability to the global modes which can lead to significant amounts of angular momentum transfer and dissipation.

In Figure 5 we plot the Toomre parameter  $Q$  as a function of radius for galaxies with a range of surface brightnesses. We have assumed that all of the galaxies have the same central radial velocity dispersion ( $\sigma_{V_r} = 100$  km/s) and constant disk thickness, as is implied by observations of edge-on LSBs (Dalcanton & Shectman 1996, Cowie et al. 1996). This leads to a radial dependence on velocity dispersion which falls like  $\exp r/2\alpha$ , as has been observed for normal galaxies (van der Kruit & Freeman 1986, Bottema 1993). With this choice of  $\sigma_{V_r}$ ,  $Q$ ’s inverse dependence on surface density leads to all models with surface densities at or below the Freeman value being stable, but leads high surface density disks, which are strongly self-gravitating, to be globally unstable over almost the entire disk.

Given the large uncertainty in the velocity dispersion  $\sigma_{V_r}$  outside of the regime of normal galaxies, we have also calculated the minimum velocity dispersion which would be needed to stabilize the disks in Figure 5. The high surface density galaxies would require velocity dispersions which were typically greater than 40% of their circular velocity in order to be stable. However, such high velocity dispersions would lead to highly non-circular orbits and thus be likely to produce angular momentum transfer and dissipation. Thus, we again expect that the high surface density disks would not take the form predicted by our models.

These very high density disks would presumably become unstable to bar formation, which can cause both central concentration and vertical heating, leading to the formation of a bulge (Combes & Sanders 1981, Pfenniger 1984, 1985, Combes et al. 1990, Pfenniger & Norman 1990, Friedli & Pfenniger 1990, Pfenniger & Friedli 1991, Raha et al. 1991). Although current numerical models for the secular formation of a bulge find it difficult to make extremely large bulges, these models usually begin with a “normal” disk, as opposed to an extremely high surface density disk such as the one in Figure 5; we would be most interested in further numerical studies of the dynamical instabilities of concentrated high surface density disks. Observationally, the lack of any significant color difference between bulges and disks, particularly in the redder bands ( $\Delta(R - K) = 0.078 \pm 0.165$ ; Peletier & Balcells 1996), as well as the correlation between disk scale length and bulge scale length (de Jong 1996, Courteau et al. 1996) and preponderance of exponential bulge profiles (Courteau et al. 1996) all support the notion that in a large fraction of galaxies, the creation of the bulge is closely tied to the formation of the disk. Of course, there are likely to be additional routes to bulge and/or elliptical formation; for a “messy” dissipative collapse, the gas may never settle into a disk at all, and entirely wind up as a condensed elliptical. Finally, our stability analysis shows that massive galaxies are more likely to be Toomre

unstable, particularly in the inner regions, which would suggest that higher mass galaxies should have a larger bulge-to-disk ratio, in general. Likewise, galaxies which form from low angular momenta halos are also more likely to be Toomre unstable, again leading to a larger bulge-to-disk ratio. This scenario suggests that the Hubble sequence might be a sequence of both mass and angular momentum.

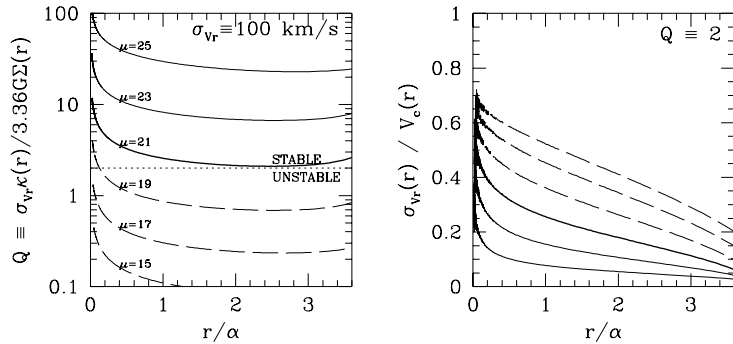


Fig. 5.—

Disk stability as a function of surface brightness. The left panel plots the Toomre stability parameter  $Q \equiv \frac{\sigma_{V_r} \kappa}{3.36 G \Sigma}$  as a function of radius (scaled by the exponential scale length  $\alpha$ ), for model disk galaxies with  $\mu_0 = 15, 17, 19, 21, 23, \& 25$   $B$  mag/arcsec $^2$  and scale lengths of 3 kpc. The model disk with a characteristic Freeman value ( $\mu_0 \sim 21$ ) is plotted as a dark line. Brighter disks are plotted as dashed lines, and the LSBs are plotted as solid lines. The models assume a radial velocity dispersion of  $\sigma_{V_r}$  which falls off radially from 100 km/s in the center such that constant disk thickness is preserved ( $\sigma_{V_r} \propto \exp -r/2\alpha$ ). The high surface brightness disks have  $Q < 2$  and are likely to be unstable. The LSBs, which are dark matter dominated, are likely to be stable. The right panel plots the minimum radial velocity dispersion needed to stabilize the disks in the top panel, assuming  $Q_{crit} = 2$ , and plotted as a fraction of the circular velocity. The high surface brightness disks (dashed lines) require radial velocity dispersions which are a large fraction of their circular velocities in order to be stable to bar formation and other large scale modes which may result in angular momentum transfer and secular bulge formation.

The predicted distribution of scale lengths and surface brightnesses in Figure 4 argues that there should be disks over a huge range of physical scale and surface brightnesses, well outside of the range of disk properties represented in large catalogs such as the NGC and UGC. There should be large numbers of both intrinsically small galaxies and low surface brightness galaxies, both of which are difficult to detect. While the photographic field surveys which have produced the largest galaxy catalogs are basically restricted to the part of the  $\alpha$ - $\mu_0$  plane occupied by the filled circles, other specialized surveys can find galaxies in other parts of the plane. For example, galaxies in the Local Group (filled triangles) and from deep surveys of the Virgo cluster are also plotted on Figure 4. These surveys clearly show that there are indeed galaxies whose properties lie well outside of the region occupied by galaxies from larger field surveys. More importantly, the cluster surveys plotted in Figure 4 (open squares and stars) do not suffer from the strong bias towards intrinsically large galaxies which affects field surveys, and more closely reflect the intrinsic distribution of scale lengths; the plotted galaxies from these surveys are almost entirely found with very small scale lengths, suggesting that there is indeed the predicted rise towards intrinsically small galaxies, as shown by the contours of  $n(\lg \alpha, \mu_0)$ . We expect the rise in the number of physically small galaxies to exist at both low and high surface brightnesses, suggesting that there may be a significant but overlooked population of very compact, high surface brightness galaxies; such galaxies would easily be mistaken for stars, and may well be as under-represented in large galaxy catalogs as the population of LSBs.

To make the above comparison between the calculated distribution of surface density and the observed distribution of surface brightness, we have assumed that all disks have a single conversion efficiency for turning gas into stars, such that there is a single disk mass-to-light ratio  $\Upsilon$ . In using a single mass-to-light ratio for all disks, we have swept a good deal of physics under the rug. In particular, we believe that our neglect of detailed physical processes within the galaxies causes us to systematically overestimate the surface brightness of LSBs, given that almost all mechanisms for reducing star formation efficiency are likely to be more effective in low surface density galaxies than in high surface density ones. First, if star formation requires a large reservoir of neutral gas, then the extragalactic ultraviolet background, which will completely ionize low surface density galaxies (§4), may suppress or shut off the formation of stars in these galaxies (Babul & Rees 1992, Efstathiou 1992). Second, if star formation is associated with the gas in disks becoming locally Toomre unstable to the formation of spiral structure (implying that the Toomre stability parameter  $Q \propto \sigma \kappa / G \Sigma$  is smaller than some constant, where  $\sigma$  is the velocity dispersion of the gas,  $\Sigma$  is the surface density of the disk, and  $\kappa$  is the epicyclic frequency, set by the disk structural parameters (see Kennicutt 1989)), then one would expect lower surface density disks to be less unstable for star formation. Observations by van der Hulst et al. (1993) find that LSB

galaxies do have HI surface densities that fall below the critical density implied by  $Q$  and are about a factor of 2 lower than the HI surface densities of HSB galaxies. Third, low surface density, low mass galaxies are more likely to lose their gas through supernova driven winds than high surface density, high mass galaxies are. The gas loss both shuts off star formation prematurely and evolves the galaxy towards larger sizes through sudden mass loss and subsequent revirialization (Dekel & Silk 1986, DeYoung & Heckman 1994, Babul & Ferguson 1996) – both mechanisms which lead to lower surface brightnesses for low surface density objects. However, because the gas loss is expected to stop when SN-driven bubbles “blow-out” the top and bottom of the disk, leaving a gas void whose width is comparable to the thickness of the disk, these effects are likely more severe in low velocity dispersion halos and may not play a role in the larger LSB disks.

In spite of these effects, for disks with central surface brightness brighter than  $\mu_0 < 24 \text{ mag/arcsec}^2$  (for the range of masses spanned by the filled circles in Figure 4) we have reason to believe that the assumption of a single value of  $\Upsilon$  is valid for the population as a whole. As discussed in §2.1.3, if  $\Upsilon$  varied systematically with surface density over this range, the mean Tully-Fisher relation in Figure 3 would shift up or down towards brighter or fainter absolute magnitudes, as a function of surface brightness. However, because the mean Tully-Fisher relation is observed to be identical for all disk galaxies with  $\mu_0 < 24 \text{ mag/arcsec}^2$  (Zwaan et al. 1995, Sprayberry et al. 1995), there cannot be significant variations in  $\Upsilon$  with surface brightness. Likewise, because the predicted slope agrees closely with the measured one, there is unlikely to be a systematic variation in  $\Upsilon$  with mass as well. Zwaan et al. (1995) do observe that the scatter in the Tully-Fisher relationship is about twice as high in LSBs as in normal galaxies, suggesting that *individual* LSB galaxies are more likely to have values of  $\Upsilon$  which depart from the mean; however, the population as a whole seems to have the same mean disk mass-to-light ratio. There may well be systematic variations in  $\Upsilon$  outside of the range of disk properties spanned by Tully-Fisher measurements; if included theoretically, the variation in  $\Upsilon$  would be manifested in Figure 4 as a vertical stretching of the contours of  $n(\alpha, \mu_0)$ .

### 3.2. Selection Effects Upon the Luminosity Function

The predicted distribution of disk scale lengths and surface brightnesses plotted in Figure 4 suggests that there are large numbers of uncataloged galaxies which have not contributed to measurements of the local luminosity function. In particular, although it is rarely discussed explicitly, most galaxy surveys are sensitive only to galaxies whose central surface brightness exceeds some minimum critical surface brightness,  $\mu_{min}$ . As can be seen

from the contour lines in Figure 4, when compared to the range of surface brightnesses covered by major field surveys ( $\mu_0 < 22 \text{ mag/arcsec}^2$  typically), the mismeasurement of the luminosity function may be severe even for bright galaxies. Furthermore, because lower mass galaxies also tend to have lower surface brightnesses, the degree of incompleteness is always worse at faint luminosities; thus a surface brightness limited sample will always underestimate the faint end slope of the galaxy luminosity function.

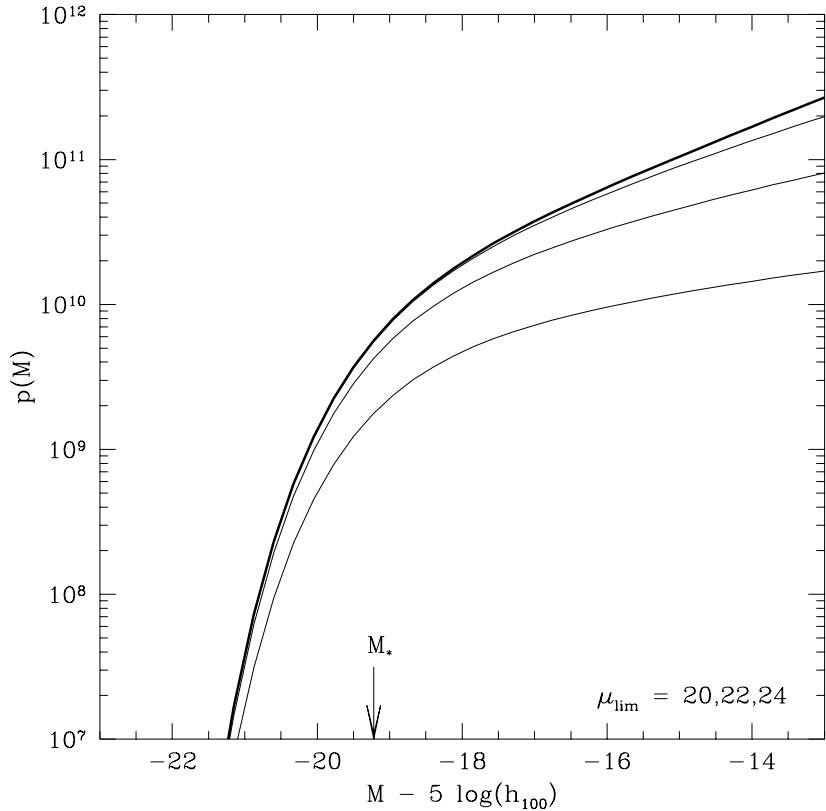


Fig. 6.—

The luminosity function which would be observed for different limiting surface brightnesses (from top to bottom,  $\mu_{lim} = \infty, 24, 22, 20 \text{ mag/arcsec}^2$ ), appropriate for a completely unbiased survey, a deep pencil beam survey, a local field survey, and a multi-fiber field survey. We have assumed an intrinsic luminosity function of the form  $p(L) \propto (L/L_*)^{-1.5} \exp(-L/L_*)$ , in arbitrary units of per luminosity per volume. Note that there is not only a significant depression of the faint end slope, but also a potentially large underestimate of the number of bright  $L_*$  galaxies. See Figure 7 for the corresponding underestimate in the luminosity density. We have assumed the same parameters as in Figure 4.

We can quantify the degree to which the limiting surface brightness of a survey leads to underestimates of the luminosity function. Equation 22 gives the distribution of surface brightness at a fixed disk mass,  $M_d$ , corresponding to a fixed disk luminosity  $L \equiv M_d/\Upsilon$ . The observed luminosity function is therefore true luminosity function weighted by the integral of equation 22 from 0 to  $\mu_{min}$ . Figure 6 shows the resulting luminosity function predicted by our model as a function of the surface brightness cutoff, assuming an underlying luminosity function  $n(L) \propto (L/L_*)^{-1.5} \exp(-L/L_*)$ . The lines correspond to different surface brightness limits, appropriate to different types of galaxy surveys; shallow multi-fiber surveys of the field (e.g. LCRS (Lin 1996)), deeper surveys of the field (e.g. CfA (Marzke et al 1994)), or deep pencil beam redshift surveys (e.g. CFRS (Lilly et al. 1996)).

First, from Figure 6 it is clear that the luminosity function can be significantly underestimated, even at  $L_*$ . The field surveys with the shallowest surface brightness limits can be missing more than a factor of 5 of bright  $L_*$  galaxies. Even deeper surveys of the local field can be missing a factor of 2. Only when surveys reach comparable depths to deep pencil beam surveys are the surveys identifying the majority of bright galaxies. This immediately has bearing on the apparent excess of “faint blue galaxies” at moderate redshifts; as pointed out by McGaugh (1994), the surface brightness selection effects are different in deep pencil beam surveys than in the local field galaxy surveys, potentially leading to the inclusion of lower surface brightness galaxies in deep surveys which are otherwise missed in tabulations of the local galaxy population. From Figure 6 it is clear that the expected magnitude of this effect is rather large, with there being 2-5 times as many bright galaxies visible in deep surveys as would be expected on the basis of measurements of the local luminosity function. We note that this is remarkably similar to the discrepancy between the observed luminosity density in deep pencil beam surveys and that which would be derived from the local field luminosity function (Dalcanton 1993).

Second, there is a systematic decrease in the observed faint end slope with brighter surface brightness limits; for an intrinsic faint end slope of  $-1.5$ , the measured slope would be  $-1.15$ ,  $-1.26$ , or  $-1.38$  for surface brightness limits of  $\mu_{min} = 20, 22$ , or  $24$ . Semi-analytic models of galaxy formation consistently predict steeper faint end slopes than are observed, but without making any correction for surface brightness selection effects (Kauffmann, White & Guiderdoni 1993; Lacey et al. 1993; Heyl et al. 1994). While this shortfall at the faint end has been seen as a failure of theories of structure formation, such as CDM, Figure 6 suggests that surface brightness selection effects are easily capable of producing the shortfall. We should also note that while theoretical predictions of the luminosity function do not tend to overestimate the number of bright galaxies, this could easily be due to choosing normalizations based upon observations of only the population of high surface brightness galaxies.

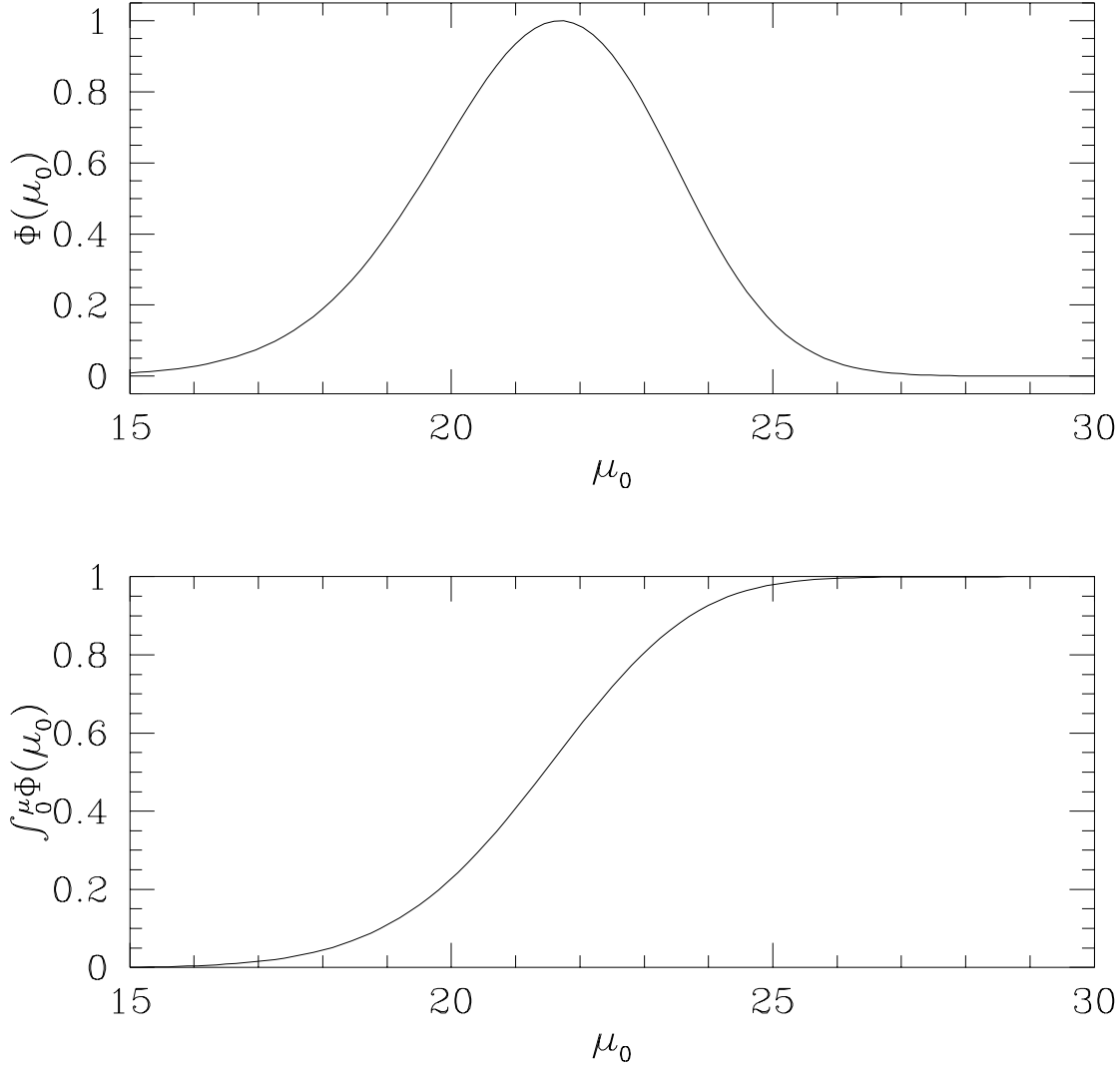


Fig. 7.—

The differential and cumulative luminosity density in arbitrary units as a function of central surface brightness (upper and lower panels respectively), assuming the same parameters as in Figures 4 & 6. Most of the luminosity density comes from galaxies with central surface brightnesses between 20 and 23 mag/arcsec<sup>2</sup> (upper panel), suggesting that current surveys are missing a significant fraction of the luminosity density of the universe. The lower panel shows that only deep surveys with  $\mu_{lim} = 25$  mag/arcsec<sup>2</sup> are capable of detecting most of the light in the universe.

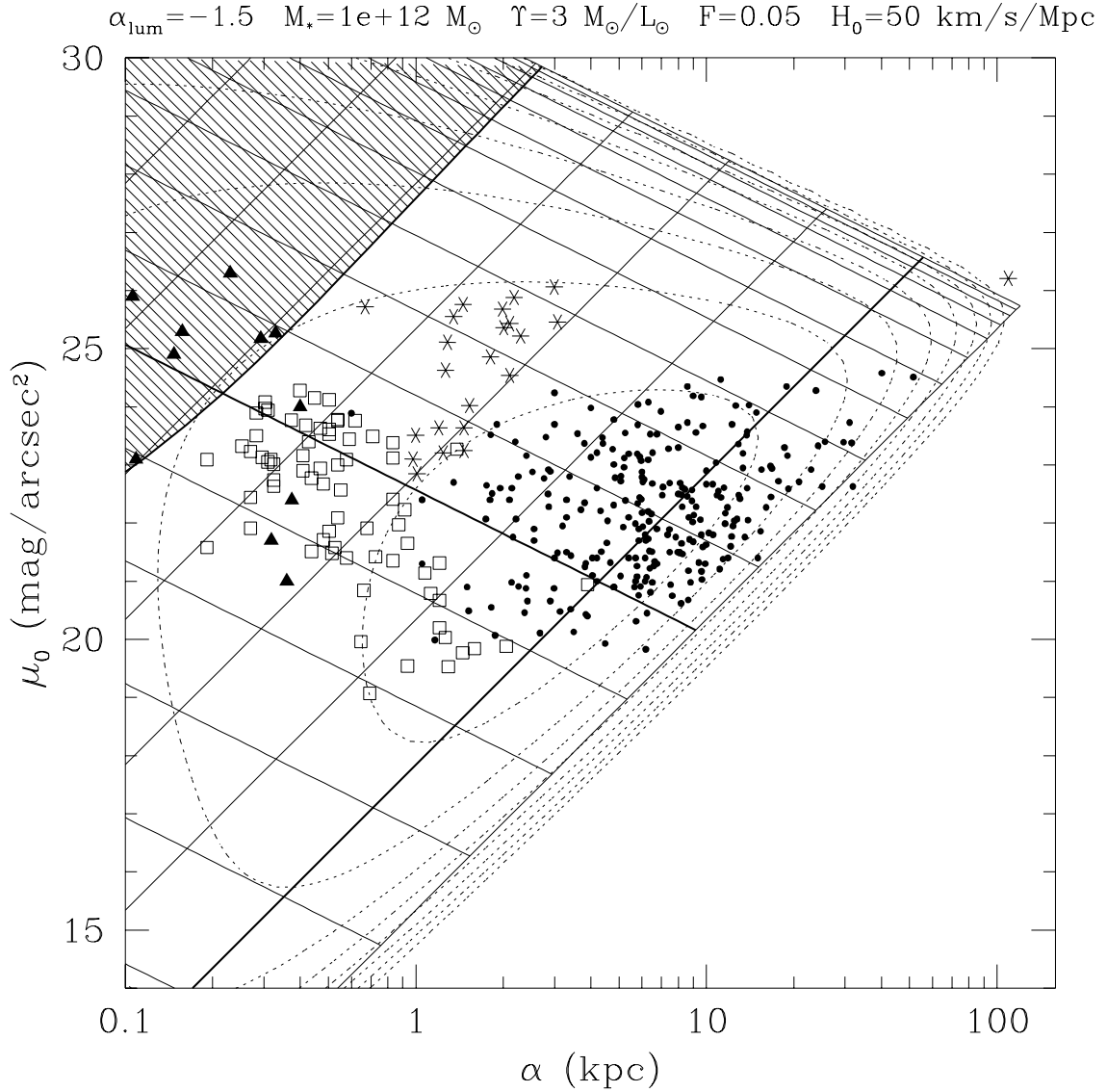


Fig. 8.—

The relative luminosity density as a function of  $B$  central surface brightness  $\mu_0$  and scale length  $\alpha$ . Identical to Figure 4, except the dotted lines are contours of constant luminosity density,  $\Phi(\lg \alpha, \mu_0)$ , separated by factors of 10.

The potentially large underestimate of the number density of galaxies suggests that current determinations of the luminosity function may also underestimate the total luminosity in galaxies. We can estimate the total luminosity density produced by disc galaxies as a function of surface brightness by integrating the intrinsic luminosity function weighted by  $p(\mu_0|L)$  (equation 22) over luminosity:

$$\phi(\mu_0) = \int_{L_{min}}^{\infty} n(L)p(\mu_0|L)LdL, \quad (27)$$

where  $L_{min} \equiv M_{min}/\Upsilon$ , from equation 19, is the expected cutoff in the galaxy luminosity function. Figure 7 shows the resulting luminosity density as a function of surface brightness, assuming a faint end slope of  $\alpha_{lum} = -1.5$ . The lower panel in the figure shows the cumulative luminosity density distribution; it suggests that only deep surveys with  $\mu_{lim} \approx 24 \text{ mag/arcsec}^2$  are capable of observing most of the luminosity density of the universe (see, e.g., Vaisanen 1996). Figure 8 shows how the relative contribution to the luminosity density changes as a function of galaxy surface brightness and scale length. From the contours of constant luminosity density, it is clear that galaxies with central surface brightness as faint as  $25 \text{ mag/arcsec}^2$  and with scale lengths as small as  $0.2 \text{ kpc}$  make significant contributions to the luminosity density of the universe.

The underestimate of the local luminosity function has strong implications for measurements of the mass density of the universe,  $\rho_0$ . One common technique to measure  $\rho_0$  is to take the local luminosity density and scale it by the large scale mass-to-light ratio measured in rich clusters such as Coma. However, if the luminosity of Coma were to be determined over a much wider surface brightness range than the local luminosity function, then the appropriate mass-to-light ratio for calculating  $\rho_0$  would be much larger than the measured mass-to-light ratio for Coma. Failing to correct for this effect could lead to measured values of  $\rho_0$  which are factors of 2 or more too low.

#### 4. Gas Detection

We have postulated that hierarchical structure formation models naturally lead to a large population of low surface brightness disk galaxies. While such a pervasive population of LSB's is difficult to detect optically, it could potentially manifest itself in blind HI surveys. However, it has often been considered a failing of hierarchical structure formation scenarios that deep HI surveys have failed to uncover a significant population of dwarf galaxies. The few uncataloged dwarfs that are discovered are preferentially found near bright galaxies (see van Gorkom 1993 for a recent review). There does not seem to be a

large population of gas rich dwarfs in the small volume which has been explored in blind HI surveys.

However, in light of recent work showing a sharp cutoff in HI disks at column densities of  $10^{19} \text{ cm}^{-1}$  (Corbelli, Schneider, & Salpeter 1989), the paucity of HI dwarfs may not be surprising. Recent work by Maloney (1993) and Corbelli & Salpeter (1993) convincingly demonstrates that ionization of the HI by a UV background accounts for the sharp cutoff in HI disks. As we have shown that low-mass galaxies tend to have low surface densities, these galaxies will be prone to having their hydrogen ionized, reducing their detectable HI masses well below their total hydrogen masses. On the other hand, HI observations of LSBs find that while the HI surface density of LSBs are less than normal galaxies, the ratio of HI mass to blue luminosity is high, suggesting that LSBs are in general less evolved than normal galaxies, due either to formation time, or to reduced star formation efficiency (van der Hulst et al. 1993, de Blok et al. 1996). This effect may partially counteract the likely decrease in the neutral fraction due to ionization. However, the ratio of HI mass to blue luminosity is only a factor of  $\approx 2$  higher than normal galaxies, while the surface brightnesses are factors of ten lower, suggesting that the two competing effects are unlikely to cancel completely.

Low surface density galaxies are therefore likely to suffer from strong biases against their detection in HI surveys, not just in optical surveys. A large population of LSB's could easily have been overlooked by existing surveys. The dwarfs that have been detected in HI surveys must have higher surface densities in general, and thus are more likely to have collapsed earlier from larger overdensities. This would explain why these dwarfs are found to trace the bright galaxy population. (For a more complete discussion of constraints on the LSB population from 21 cm surveys, see McGaugh (1996).) However, while the neutral gas fraction of LSBs may be small enough to keep them out of surveys of HI emission, they may well be seen in absorption, particularly in the Lyman- $\alpha$  forest.

## 5. Summary

In this paper, we have developed a scenario that links the mass and angular momentum of a proto-galaxy to the luminosity and surface brightness of the resultant galactic disk. Gas in low angular momentum proto-galaxies collapse by large factors to form high surface brightness galaxies. Low surface brightness galaxies form from low mass and high angular momentum proto-galaxies.

As gravitational collapse in any hierarchical model with Gaussian initial conditions leads to a broad distribution of halo masses and angular momentum, we expect that galaxies

should have a wide range of surface brightness and disk scale lengths. We expect that some disk galaxies form with surface brightnesses less than  $27 B \text{ mag/arcsec}^2$ , well below current observational limits. We also expect the number density of galaxies to rise towards small scale lengths and low surface brightnesses, as is seen in surveys of nearby clusters. This correlation also leads to an apparent correlation between surface brightness and magnitude, as is observed (Bingelli et al. 1984, Ferguson & Sandage 1988).

Following Mestel (1963), Fall & Efstathiou (1980), Gunn (1982), van der Kruit (1987), we follow the collapse of a uniform gas cloud that has experienced a uniform external torque. We extend the earlier work by calculating the collapse in a realistic dark matter halo and use the adiabatic approximation developed by Blumenthal et al. (1986) to model the response of the halo to the disk. This scenario produces galaxy disks with asymptotically flat rotation curves and exponential light profiles, where the disk scale length is roughly proportional to  $\lambda M^{1/3}$ . Here,  $\lambda$  is the spin parameter of the proto-galaxy and  $M$  is its mass. This relation leads to galaxies that obey the Tully-Fisher law as  $v_c^2 \propto M(r_d)/r_d \propto M^{2/3} \propto L^{2/3}$ . It also helps explain the disk-halo conspiracy (Bahcall & Casertano 1985) associated with featureless rotation curves as both the disk and halo scale lengths are proportional to  $M^{1/3}$ .

The shape of the rotation curve depends upon a galaxy’s angular momentum. Low angular momentum disks are centrally concentrated and dominate the inner portions of the rotation curve. Thus, these galaxies have rapidly rising rotation curves in the centers. High angular momentum disks have their mass spread out to larger radii, leading to a smaller dynamical contribution from the disk, relative to the halo, at all radii. Thus, high angular momentum disks, which tend to be low surface brightness, have more slowly rising rotation curves. Low surface brightness disks also have apparently higher dynamical mass-to-light ratios, because their extended disks encompass a larger fraction of the dark matter halo within their optical radius. Because the disk makes a relatively small contribution to the galactic potential in LSBs, it serves as an excellent tracer of the initial dark mass profile and the shape of the dark halo. Furthermore, at a given mass, low surface brightness galaxies have much larger scale lengths, allowing them to probe the halo at much larger radii.

This model predicts that very low angular momentum proto-galaxies collapse to form very high surface brightness galaxies. Since these very high surface brightness galaxies are globally unstable to non-axisymmetric perturbations, they likely form bars, bulges and/or ellipticals. Thus, the Toomre instability criterion may explain why few disk galaxies have central surface brightnesses above the canonical Freeman value.

Our model suggests that current galaxy surveys are missing a significant fraction of the total number of galaxies, and have severely underestimated the faint end slope, due to surface brightness limits which prevent them from finding low surface brightness galaxies.

The luminosity density of the universe is similarly underestimated. The underestimate should be much less in deep pencil beam redshift surveys, and is of the right magnitude to explain much of the apparent “excess” in the galaxy population at moderate redshifts. It is intriguing that wide-field faint searches for LSBs (Dalcanton et al. 1997) are finding the large number of LSBs predicted by this model.

The galaxy formation scenario makes a number of assumptions that require further observational and numerical testing, namely: (1) that gravitational collapse leads to a universal dark matter halo (Navarro et al. 1996); (2) that angular momentum is conserved through galaxy collapse and (3) that the initial angular momentum distribution is similar to that produced by an external tidal torque. All three of these assumptions are controversial. However, wherever possible, we have shown that our results are well supported by existing observations. The success of our model in matching the observations suggests that, in spite of the simplicity of our assumptions, the overall scenario merits careful examination.

#### Acknowledgements

We thank Arif Babul, John Bahcall, Daniel Eisenstein, Jim Gunn, and Ian Smail for useful discussions, and the referee, P. C. van der Kruit for very helpful suggestions. DNS was supported by NASA. Support for JJD was provided by NASA through Hubble Fellowship grant #2-6649 awarded by the Space Telescope Science Institute, which is operated by the Association of Universities for Research in Astronomy, Inc., for NASA under contract NAS 5-26555.

## 6. References

Allen, R. J., & Shu, F. H. 1979, *Ap. J.*, 227, 67.

Athanassoula, E. 1984, *Physics Reports*, 114, 321.

Babul, A. 1989, Ph.D. thesis, Princeton University.

Babul, A., & Ferguson, H. C. 1996, *Ap. J.*, 458, 100.

Babul, A., & Rees M. J. 1992, *M.N.R.A.S.*, 255, 346.

Bahcall, J.N. & Casertano, S. 1985, *Ap. J.*, 293, L7.

Barnes, J. E., & Efstathiou, G. 1987, *Ap. J.*, 319, 575.

Bender, R., Burstein, D. & Faber, S.M. 1992, *Ap. J.*, 399, 462.

Bernstein, G. M., Tyson, J. A., Brown, W. R., & Jarvis, J. F. 1993, *Ap. J.*, 426, 516.

Bernstein, G.M., et al. 1994, *A. J.*, 107, 1962.

Bingelli, B., Sandage, A., & Tarenghi, M. 1984, *A. J.*, 89, 64.

Blumenthal, G. R., Faber, SM, Flores, R & Primack, JR 1986 *Ap. J.*, 301, 27.

Bond, J. R., Cole, S., Efstathiour, G. & Kaiser, N. 1991, *Ap. J.*, 379, 440.

Boroson, T. 1981, *Ap. J. Suppl.*, 46, 177.

Bothun, G. D., Beers, T. C., Mould, J. R., & Huchra, J. P. 1986, *Ap. J.*, 308, 510.

Bothun, G. D., Impey, C. D., & Malin, D. F. 1991, *Ap. J.*, 376, 404.

Bothun, G. D., Impey, C. D., Malin, D. F., & Mould, J. 1987, *A. J.*, 94, 23.

Bothun, G. D., Schombert, J. M., Impey, C. D., Sprayberry, D., & McGaugh, S. S. 1993, *A. J.*, 106, 530.

Bottema, R. 1993, *Astr. Ap.*, 275, 16.

Bower, R. J. 1991, *M.N.R.A.S.*, 248, 332.

Burstein, D., & Rubin, V. C. 1985, *Ap. J.*, 297, 423.

Caldwell, N., Armandroff, T. E., Seitzer, P., & Da Costa, G. S., 1992 *A. J.*, 103, 840.

Catelan, P. & Theuns, T. 1996a, to appear in *M.N.R.A.S.*, .

Catelan, P. & Theuns, T. 1996b, *astro-ph/9604078*.

Cayatte, V., Kotanyl, C., Balkowski, C., & van Gorkom, J. H. 1994, *A. J.*, 107, 1003.

Combes, F. & Sanders, R. H. 1981, *Astr. Ap.*, 96, 164.

Combes, F., Debbasch, F., Friedli, D., & Pfenniger, D. 1990, *Astr. Ap.*, 233, 82.

Corbelli, E. & Salpeter, E. 1993, *Ap. J.*, 419, 104.

Corbelli, E., Schneider, S. E., & Salpeter, E. 1989, *A. J.*, 97, 390.

Courteau, S., de Jong, R. S., & Broeils, A. H. *Ap. J. (Letters)*, 457, L73.

Cowie, L. L., Hu, E. M., & Songaila, A., 1996, *A. J.*, submitted (CHS).

Dalcanton, J. J. 1993, *Ap. J. (Letters)*, 415, L87.

Dalcanton, J. J. 1995, Ph.D. Thesis, Princeton University.

Dalcanton, J. J., Spergel, D. N., Gunn, J. E., Schmidt, M., & Schneider, D. P. 1997 *A. J.*, , submitted.

Dalcanton, J. J. & Shectman, S. A. 1996, *Ap. J. (Letters)*, 465, L9.

Davis, M., Efstathiou, G., Frenk, C., & White, S. 1985, *Ap. J.*, 292, 371.

Davies, J. I., Phillipps, S., & Disney, M. J. 1988, *M.N.R.A.S.*, 231, 69P.

Davies, J. I., Phillipps, S., & Disney, M. J. 1990, *M.N.R.A.S.*, 244, 385.

de Blok, W. J. G., van der Hulst, J. M., & Bothun, G. D. 1995, *M.N.R.A.S.*, 274, 235.

de Blok, W. J. G., McGaugh, S. S., & van der Hulst, J. M. 1996, *M.N.R.A.S.*, , in press.

de Jong, R. S. 1995, Ph.D. Thesis, University of Groningen.

de Jong, R. S., & van der Kruit 1994, *Astr. Ap. Suppl.*, 106, 451.

de Jong, R. S., 1996, *Astr. Ap. Suppl.*, , 118, 557.

Dekel, A., & Silk, J. 1986, *Ap. J.*, 303, 39.

DeYoung, D., & Heckman, T. 1994, *Ap. J. (Letters)*, 431, 598.

Disney, M. 1976, *Nature*, 263, 573.

Dubinski, J. & Carlberg, R.G. 1991, *ApJ* 378, 496.

Eisenstein, D. J., & Loeb, A. 1995, *Ap. J.*, 439, 520.

Eisenstein, D. J. 1996, Harvard Ph.D. Thesis.

Efstathiou, G. 1992, M.N.R.A.S., 256, 43p.

Efstathiou, G. & Silk, J. 1983, Fund. Cos. Phys., 9, 1.

Efstathiou, G., Bernstein, G., Katz, N., Tyson, J. A., & Guhathakurta, P. 1991, Ap. J. (Letters), 380, L47.

Evrard, A. E., Summers, F. J., & Davis, M. 1994, Ap. J., 422, 11.

Faber, S. M. 1982, in *Astrophysical Cosmology*, ed. H. A. Bruck, G. V. Coyne, & M. S. Longair, (Vatican: Pontificia Acadamia Scientiarum), 191.

Ferguson, H. C., & McGaugh S. S. 1995, Ap. J., 440, 470.

Ferguson, H. C., & Sandage, A. 1988, A. J., 96, 1520.

Flores, R., Primack J. R., Blumenthal, G. R., & Faber, S. M. 1993, Ap. J., 412, 443.

Freeman, K. C. 1970, Ap. J., 160, 811.

Gallagher, J. S., & Hunter, D. A. 1984, Ann. Rev. Astr. Ap., 22, 37.

Gnedin, O., Goodman, J., & Frei, Z. 1985, A. J., 110, 1105.

Goad, J. W., & Roberts, M. S. 1981, Ap. J., 250, 79.

Gunn, J. E. 1982, in *Astrophysical Cosmology*, ed. H. A. Bruck, G. V. Coyne, & M. S. Longair, (Vatican: Pontificia Acadamia Scientiarum), 191.

Heyl, J. S., Cole, S., Frenk, C. S., & Navarro, J. F. 1994, astro-ph/9408065.

Hoffman, Y., Silk, J., Wyse, R. F. G. 1992, Ap. J. (Letters), 388, L13.

Impey, C. D., Bothun, G. D., & Malin, D. F. 1988, Ap. J., 330, 634.

Impey, C. D., Sprayberry, D., Irwin, M., & Bothun, G. D. 1996, Ap. J. Suppl., 105, 209.

Irwin, M. J., Davies J. I., Disney, M. J., & Phillips, S. 1990, M.N.R.A.S., 245, 289.

Jeans, J. H. 1929, *Astronomy and Cosmogony*, 2nd ed., (Cambridge, England: Cambridge University Press).

Kaiser, N. 1984, Ap. J. (Letters), 284, L9.

Katz, N., & Gunn, J. E. 1991 Ap. J., 377, 365.

Kauffmann, G., White, S.D.M. & Guiderdoni, B. 1993, M.N.R.A.S., 264, 201.

Kennicutt, R. C. 1989, Ap. J., 344, 685.

Koo, D. C., & Szalay, A. 1984, *A. J.*, 282, 390.

Knezek, P. 1993, Ph.D. Thesis, University of Massachusetts.

Lacey, C., & Cole, S. 1993, *M.N.R.A.S.*, 262, 627.

Lacey, C., Guiderdoni, B., Rocca-Volmerange, B. & Silk, J. 1993, *Ap. J.*, , 402, 15.

Lilly, S. J., Tresse, L., Hammer, F., Crampton, D., & Le Fevre, O. 1995, *Ap. J.*, 455, 108.

Lin, H., Kirshner, R. P., Shectman, S. A., Landy S. D., Oemler, A., Tucker, D. L., & Schechter, P. L. 1996, *Ap. J.*, submitted.

Lo, K. Y., Sargent, W. L. W., & Young, K. 1993, *A. J.*, 106, 507.

Loveday, J., Peterson, B. A., Efstathious, G., Maddox, S. J. 1992, *Ap. J.*, 390, 338.

Maloney, P. 1993, *Ap. J.*, , 414, 41.

McGaugh, S. S., & Bothun, G. D. 1994, *A. J.*, 107, 530.

McGaugh, S. S. 1994, *Ap. J.*, 426, 135.

McGaugh, S. S. 1994, *Nature*, 367, 538.

McGaugh, S. S. 1996, *M.N.R.A.S.*, 280, 337.

McGaugh, S. S., Schombert, J. M., & Bothun, G. D. 1995, *A. J.*, 109, 2019.

Mestel, L. 1963 *M.N.R.A.S.*, 126, 553.

Mo, H. J., McGaugh, S. S., & Bothun, G. D. 1994, *M.N.R.A.S.*, 267, 129.

Mo, H. J. & White, S. D. M. 1995, submitted to *M.N.R.A.S.*, , astro-ph/9512127.

Navarro, J.F., Frenk, C.S. & White, S.D.M. 1996, *Ap. J.*, 462, 563.

Navarro, J.F., & Steinmetz, M., 1996, astro-ph/9605043.

Navarro, J.F., & White, S.D.M., 1993, *M.N.R.A.S.*, 265, 271

Nilson, P. 1973, Uppsala General Catalog of Galaxies, Uppsala Astr. Obs. Ann., Vol.6.

Ostriker, J. P. & Peebles, P. J. E. 1973, *Ap. J.*, , 186, 487.

Peacock, J. & Heavens A. 1989, *M.N.R.A.S.*, 243, 133.

Peebles, P. J. E. 1969, *Ap. J.*, 155, 393.

Persic, M., & Salucci, P. 1995, *Ap. J. Suppl.*, 99, 501.

Persic, M., Salucci, P., & Stel, F. 1996, M.N.R.A.S., 281, 27.

Pfenniger D. 1984, Astr. Ap., 134, 373.

Pfenniger D. 1985, Astr. Ap., 150, 112.

Pfenniger D., & Norman, C. 1990, Ap. J., 363, 391.

Pfenniger D., & Friedli, D. 1991, Astr. Ap., 252, 75.

Phillipps, S., Davies, J. I., & Disney, M. J. 1990, M.N.R.A.S., 242, 235.

Press, W. H., & Schechter, P. L. 1974, Ap. J., 330, 579.

Pritchett C. J., & Infante L. 1992, Ap. J. (Letters), 399, L35.

Quinn, T. & Binney, J. 1992, MNRAS, 255, 729.

Raha N., Sellwood, J. A., James, R. A., & Kahn, F. D. 1991, Nature, 352, 411.

Ryden, B.S. 1988, ApJ, 329, 589.

Romanishin, W., Strom, K. M., & Strom, S. E. 1983, Ap. J. Suppl., 53, 105.

Schechter, P. 1975, Caltech Ph.D. Thesis.

Schombert, J. M., & Bothun, G. D. 1988, A. J., 95, 1389.

Schombert, J. M., Bothun, G. D., Schneider, S. E., & McGaugh, S. S. 1992, A. J., 103, 1107

Shapiro, P. R., Giroux, M. L., & Babul, A. 1994, Ap. J., 427, 25.

Shectman, S. A. 1974, Ap. J., 188, 233.

Sprayberry, D., Bernstein, G. M., Impey, C. D., & Bothun, G. D. 1995a, Ap. J., 438, 72.

Sprayberry, D., Impey, C. D., Bothun, G. D., Irwin, M. J. 1995b, A. J., 109, 558.

Sprayberry, D., Impey, C. D., & Irwin, M.J. 1996, Ap. J., 463, 535

Stevenson, P. R. F., Shanks, T., Fong, R., & MacGillivray, H. T. 1985, M.N.R.A.S., 213, 953.

Strauss, M. A., & Willick, J. A. 1995, Phys. Rep. 261, 271.

Toomre, A. 1964, Ap. J., 139, 1217.

Tully, R. B., & Fisher J. R. 1977, Astr. Ap., 54, 661.

Turner, J. A., Phillips, S., Davies, J. I., & Disney, M. J. 1993, M.N.R.A.S., 261, 39.

Vaisanen, P. 1996, CfA preprint 4308 (astro-ph/9604147), to appear in *Astr. Ap.*,  
van der Hulst, J. M., Skillman, E. D., Smith, T. R., Bothun, G. D., McGaugh, S. S., & de  
Blok, W. J. G. 1993, *A. J.*, 106, 548.

van der Kruit, P. C. 1987 *AA* 173, 59.

van der Kruit, P. C. & Freeman, K. C. 1986, *Ap. J.*, 303, 556.

Warren, M. S., Quinn, P. J., Salmon, J. K., & Zurek, W. H. 1992, *Ap. J.*, 399, 405.

White, S. D. M. 1994, MAP preprint.

White, S. D. M., David, M., Efstathiou, G., & Frenk, C. S. 1987, *Nature*, 330, 451.

White, S. D. M., & Frenk, C. S. 1991, *Ap. J.*, 379, 52.

Willick, J. A., Courteau, S., Faber, S. M., Burstein, D., Dekel, A., & Kolatt, T. 1996,  
*Ap. J.*, 457, 460.

Willick, J. A., Courteau, S., Faber, S. M., Burstein, D., & Dekel, A. 1995, *Ap. J.*, 446, 12.

Zhang, X. 1996, *Ap. J.*, 457, 125.

Zwaan, M. A., van der Hulst, J. M., de Blok, W. J. G., & McGaugh, S. S. 1995, M.N.R.A.S.,  
273, L35.

Zwicky, F. 1957, in *Morphological Astronomy*, (New York: Springer-Verlag).

## 7. Appendix

In this appendix, we redo the calculation presented in the main text, but here model the initial halo density distribution as  $\rho(r) = B\rho_0 r_0 / [r_i(1+r_i^2/r_0^2)]$ . This density distribution is close to that fit by Navarro, Frenk and White (1996) to their numerical simulations. In their simulations,  $B \simeq 7 \times 10^4$ , and the density profile extends to  $r_{\max} \simeq 7.4r_0$ . The mass profile that corresponds to the initial dark halo mass distribution can be inverted:

$$r_i = r_0 \sqrt{\left(1 + \frac{r_{\max}^2}{r_0^2}\right)^{m_h} - 1} \quad (28)$$

As in section 2, we can calculate the final radial distribution of the disk and the halo by requiring angular momentum conservation:

$$m_d = 1 - \left[ 1 - \beta m_h^{1/2} \sqrt{\left(1 + \frac{r_{\max}^2}{r_0^2}\right)^{m_h} - 1} \right]^{3/2} \quad (29)$$

$$r_f = \frac{m_h r_0 \sqrt{\left(1 + \frac{r_{\max}^2}{r_0^2}\right)^{m_h} - 1}}{(1 - F)m_h + Fm_d} \quad (30)$$

where  $\beta = \sqrt{G(1 - F)M_{\text{tot}}}/J_{\max}$ . For  $r_{\max} = 7.4r_0$ , the energy of the halo is  $-0.085GM_{\text{tot}}^2/r_0$ , thus,  $r_0 = 0.141a$ , where  $a$  is the radius of the initial fluctuation that collapsed to form the galaxy. Hence,  $\beta \simeq 0.15/\lambda$ . Figure 9 shows the rotation curves and surface density profiles for a range of values for  $\lambda$  and  $F$ . For this model, the disk scale length,  $r_{\text{disk}} \simeq a\lambda^b r_0$ , where  $a = 4.6 * (1 + 20f)$  and  $b = 1 + 6f$

Following the same approach used in sections 2 and 3, we can compute the predicted distribution of surface densities at a given luminosity:

$$p(\mu_0|L) = \frac{\delta}{1.08b\sqrt{2\pi}} \exp\left[-\frac{(\mu_0 - \bar{\mu}(L))^2}{2(1.08\delta)^2 b^2}\right] d\mu_0 \quad (31)$$

where

$$\bar{\mu}(L) = -2.5 \log_{10} \left[ \frac{B^2}{2\pi a^2} \left( \frac{F\rho_0}{\Upsilon} \right)^{2/3} \frac{L^{1/3}}{\langle \lambda \rangle^{2b}} \right] = \mu_* + \frac{5}{6} \log_{10} \left( \frac{L}{L_*} \right) \quad (32)$$

This model yields similar predictions to the Hernquist model used in the main text; however, now the width of the central surface density distribution is slightly broader:  $\sigma_{disk} = 1.08\delta(1 + 6f)$ .

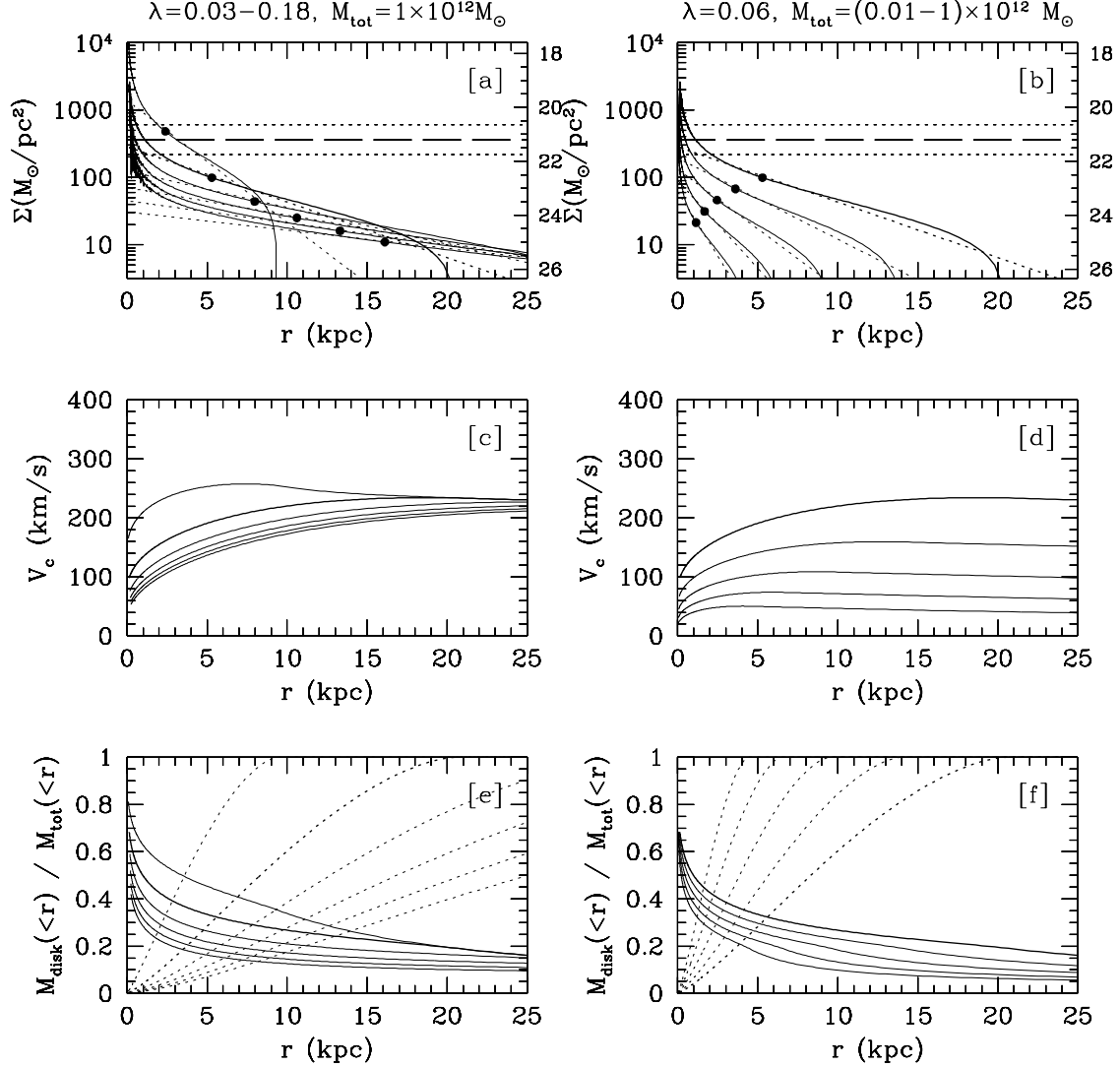


Fig. 9.—

Same as Figure 1, but for an initial halo density profile of the form:  $\rho(r_i) \propto r_i^{-1}(r_i^2 + r_0^2)^{-1}$